J. Fluid Mech. (2001), *vol.* 449, *pp.* 341–371.
DOI: 10.1017/S0022112001006139 Printed in the United Kingdom

Numerical modelling of water-wave evolution based on the Zakharov equation

By SERGEI YU. ANNENKOV[1] AND VICTOR I. SHRIRA[2]

[1]P. P. Shirshov Institute of Oceanology, Russian Academy of Sciences,
36 Nakhimovsky prosp., Moscow 117851, Russia
e-mail: serge@wave.sio.rssi.ru

[2]Department of Mathematics, Keele University, Keele ST5 5BG, UK
e-mail: v.i.shrira@maths.keele.ac.uk

(Received 22 February 2001 and in revised form 11 July 2001)

We develop a new approach to numerical modelling of water-wave evolution based on the Zakharov integrodifferential equation and outline its areas of application.

The Zakharov equation is known to follow from the exact equations of potential water waves by the symmetry-preserving truncation at a certain order in wave steepness. This equation, being formulated in terms of nonlinear normal variables, has long been recognized as an indispensable tool for theoretical analysis of surface wave dynamics. However, its potential as the basis for the numerical modelling of wave evolution has not been adequately explored. We partly fill this gap by presenting a new algorithm for the numerical simulation of the evolution of surface waves, based on the Hamiltonian form of the Zakharov equation taking account of quintet interactions. Time integration is performed either by a symplectic scheme, devised as a canonical transformation of a given order on a timestep, or by the conventional Runge–Kutta algorithm. In the latter case, non-conservative effects, small enough to preserve the Hamiltonian structure of the equation to the required order, can be taken into account. The bulky coefficients of the equation are computed only once, by a preprocessing routine, and stored in a convenient way in order to make the subsequent operations vectorized.

The advantages of the present method over conventional numerical models are most apparent when the triplet interactions are not important. Then, due to the removal of non-resonant interactions by means of a canonical transformation, there are incomparably fewer interactions to consider and the integration can be carried out on the slow time scale ($O(\varepsilon^2)$, where ε is a small parameter characterizing wave slope), leading to a substantial gain in computational efficiency. For instance, a simulation of the long-term evolution of 10^3 normal modes requires only moderate computational resources; a corresponding simulation in physical space would involve millions of degrees of freedom and much smaller integration timestep.

A number of examples aimed at problems of independent physical interest, where the use of other existing methods would have been difficult or impossible, illustrates various aspects of the implementation of the approach. The specific problems include establishing the range of validity of the deterministic description of water wave evolution, the emergence of sporadic horseshoe patterns on the water surface, and the study of the coupled evolution of a steep wave and low-intensity broad-band noise.

1. Introduction

Numerical simulations are increasingly used for the study of nonlinear free-surface motions. The great variety of problems and assumptions relevant to the physical properties involved require various numerical methods with corresponding underlying approximations.

Early efforts in this direction were centred around attempts at the direct integration of the primitive equations of motion, with the use of boundary-discretization or volume-discretization methods (see e.g. the recent review by Tsai & Yue 1996). In the context of potential flow, considerable success has been achieved by employing the mixed Eulerian–Lagrangian (MEL) formulation of the boundary integral equation approach (e.g. Longuet-Higgins & Cokelet 1976), the Cauchy-type integral algorithm (Dold & Peregrine 1986; Dold 1992), or conformal mapping techniques (e.g. Chalikov & Sheinin 1996, 1998). This line proved to be extremely fruitful in studying the evolution of steep waves up to overturning. However, in general these methods are applicable to two-dimensional waves only, which is very restrictive. While the MEL approach can be extended to three dimensions, the overwhelming demand of computational resources all but prohibited, up to the very recent time, its application to problems dealing with three-dimensional aspects of water wave evolution (Tsai & Yue 1996).

Meanwhile, many problems of the evolution of surface waves allow one to assume the relative smallness of wave steepness, so that its explicit utilization as a small parameter appears to be appropriate. This gave rise to a number of numerical methods based on the perturbation expansion. Development of high-order spectral methods (Dommermuth & Yue 1987; West *et al.* 1987) was particularly fruitful and has led to numerous applications.

These numerical studies brought substantial progress in the understanding of the evolution of waves of small and moderate steepness. At the same time, these methods contain a number of limitations significantly restricting the range of their application.

All the existing methods for the three-dimensional simulation of water-wave evolution are based on the representation of physical variables (say, the surface elevation and potential on the surface) as Fourier series in horizontal directions and the subsequent use of fast Fourier transforms (FFT) to quickly project between the wavenumber and physical space at each step of the algorithm. In two horizontal dimensions, this technique gives satisfactory efficiency for a moderate number of degrees of freedom. However, the numerical implementation of FFT prescribes the use of rectangular grids in the initial discretization. In order to get the sufficiently high resolution necessary to capture the narrow resonance zones in most physical problems, a large and refined rectangular grid is often needed, leading to excessive requirements for computational resources. In particular, a study of statistical properties of wave turbulence through its direct simulation is so far impossible. More importantly, a rectangular (and, more generally, any integer) grid leads to undesirable artefacts, which can significantly influence the nonlinear evolution (Kartashova 1992), limiting the applicability of the results.

On the other hand, the computations, performed both in physical and Fourier space, crucially depend on the assumption that the water surface is single-valued. Provided that the initial steepness exceeds a certain (rather low) threshold, evolution in a generic case leads to local steepening and eventual overturning of waves, which means the failure of the numerical simulation at a certain time. It is important to note that for many applications, these local breaking effects play a relatively minor physical

role and can be ignored; however, the formal breakdown of the algorithm in this case necessitates a certain *ad hoc* smoothing technique that destroys the mathematical consistency of the algorithm and constitutes a separate computational problem. Note also that at present the existing algorithms for water-wave simulation employ conventional methods of integration in time, ignoring the Hamiltonian nature of the underlying theory (although the necessity of more appropriate symplectic methods of integration for water-wave problems has long been recognized (West 1992)).

Finally, the existing weakly nonlinear numerical methods, even if they are capable of reproducing specific physical phenomena, often do not reveal the physical mechanisms responsible for their emergence. In other words, the procedure of a numerical solution remains to a large extent a 'black box' from the physical viewpoint.

Meanwhile, there exists a different approach to the formulation of weakly nonlinear surface wave dynamics. In 1968, V. E. Zakharov (see Zakharov 1968), considering resonant interactions within a continuous spectrum of gravity waves, derived, as an intermediate step, the reduced integrodifferential equation for the slow evolution of a weakly nonlinear wave field. This equation, subsequently derived in more systematic manner and extended to the next order by Krasitskii (1994), governs the evolution of the complex function $b(\boldsymbol{k}, t)$, $\boldsymbol{k}$ being a wavevector and t time, obtained from physical variables by means of a canonical transformation that eliminates the non-resonant interaction terms. As is well-known, for gravity waves on the surface of deep water only quartet and higher-order resonant interactions are permitted. The Hamiltonian, being a functional of $b(\boldsymbol{k}, t)$, is diagonalized by this canonical transformation to the first nonlinear order in wave steepness, so that the function $b(\boldsymbol{k}, t)$ serves as a *nonlinear normal variable* for the Hamiltonian. From another viewpoint, this transformation can be interpreted as the elimination of all slave modes of the system, reformulating the problem in terms of master modes only. In this way, the equation obtained represents a substantial simplification with respect to the original hydrodynamic equations, since with the elimination of non-resonant interactions much of the complexity is transferred into constant coefficients (that have very cumbersome algebraic form).

Although the idea of a numerical scheme based on the Zakharov equation seems natural (Craik 1985), attempts at its implementation were rare, in contrast to the increasing popularity of spectral methods. In fact, it is fair to say that the Zakharov equation, nonetheless commonly considered as an important theoretical model of water-wave evolution, has been overlooked as a basis for the numerical investigation, being often regarded as not suitable for this purpose.

Nevertheless, the Zakharov equation has important advantages from the point of view of numerics. First, due to the fact that there are incomparably fewer interactions to consider, an algorithm based on the reduced equation will be, in theory, superior in its efficiency to any other (non-reduced) model. We note that this enormous advantage of the Zakharov approach has never been explicitly utilized, to our knowledge, for numerical simulation of water-wave problems.

Second, the Zakharov equation has the Hamiltonian form and from the symmetries perspective is equivalent to the exact equations of potential motions of the free surface (provided that the necessary number of terms is taken into account), so that the construction of a symplectic algorithm is, in principle, straightforward.

Third, since all the computations are to be carried out in the Fourier-transformed space, there is no need to perform the fast Fourier transform at each timestep, as one has to do with spectral methods. This allows us to avoid the restriction to whole-number grids.

Fourth, in contrast to all conventional methods, the Zakharov equation operates in

terms of nonlinear normal variables on the slow time scale ($O(\varepsilon^2)$, where ε is a small parameter characterizing wave slopes), widely separating the time scales and leading to substantial gain in computational efficiency.

Finally, the algorithm based on the Zakharov equation is physically the most transparent: one can easily identify the resonantly interacting modes, which are the true normal modes of the nonlinear problem to $O(\varepsilon^2)$. It enables one to separate the role of various physical factors (for instance, it is possible to consider separately the four-wave and five-wave interactions).

As much of the complexity of the original hydrodynamic equations is absorbed into cumbersome constant coefficients of the Zakharov equation, the calculation of these coefficients becomes the most time-consuming part of the computation. Thus, it is reasonable to construct an algorithm where these coefficients would be computed only once, before the application of the numerical time integration scheme, and stored in a convenient way in order to make the subsequent operations vectorized.

However, an implementation of the algorithm based on the reduced equation meets a number of substantial difficulties. In the past few decades, there have been only a few attempts to use it for numerical analysis of gravity wave evolution.

The first attempt at the numerical solution of the Zakharov equation was carried out in Caponi, Saffman & Yuen (1982) (see also Yuen & Lake 1982). Seven two-dimensional modes were taken, in the form of a carrier $\boldsymbol{k} = (k_0, 0)$ and three pairs of initially small sidebands $\boldsymbol{k}_m = (k_0 \pm m\Delta k, 0)$, $m = 1, 2, 3$, and the evolution in time was obtained for a number of values of initial carrier steepness. These authors noted that the Zakharov equation, as it was proposed in Zakharov (1968), was non-Hamiltonian, despite the Hamiltonian nature of the underlying hydrodynamic theory, so that the conservation of energy and other integrals in the computations was not ensured. The Hamiltonian version of the equation was proposed by Zakharov in his comments to the Russian edition of Yuen & Lake (1982). Later, the numerical solution to the analogous problem was given in Krasitskii & Kalmykov (1993), where the first comparison of Hamiltonian and non-Hamiltonian versions of the equation was provided.

In the original form of Zakharov (1968), the equation included only terms of $O(\varepsilon^3)$, while the higher-order processes were omitted. However, it is well-known that taking account of five-wave interactions, of $O(\varepsilon^4)$, can be essential for certain water-wave problems. The extension of the non-Hamiltonian form of the equation to the next order was carried out by Stiassnie & Shemer (1984). These authors (Shemer & Stiassnie 1985; Stiassnie & Shemer 1987) also considered numerically several examples of the evolution for the carrier, one pair of two-dimensional sidebands $\boldsymbol{k}_{1,2} = (k_0 \pm p, 0)$ and a pair of three-dimensional ones $\boldsymbol{k}_{3,4} = (\frac{3}{2}k_0, \pm q)$, where the values of p and q were taken to ensure the maximal initial growth of the satellites. Recently, Shemer *et al.* (2001) performed a number of computations of the spatial version of the Zakharov equation, comparing results with the experiments on wave evolution along a tank.

Krasitskii (1994) rederived the Zakharov equation in a systematic way up to $O(\varepsilon^4)$ within the framework of Hamiltonian theory, using the canonical transformation technique. This particular form of the equation is used in the present paper as the basis for the numerical algorithm of water-wave evolution.

For the purpose of computations, the Zakharov equation must be properly discretized. In particular, initial conditions for physical-space variables must be converted, by means of the canonical transformation and discretization in $\boldsymbol{k}$-space, to a finite set of complex amplitudes $b(\boldsymbol{k}_j)$, $j = 0, \ldots, N$ that represent the initial conditions for the subsequent integration in time. It is important to note that the set

of N wavevectors under consideration must constitute an isolated system of four- and five-wave resonances (Shrira, Badulin & Kharif 1996), in the sense that there are no harmonics that are in four- or five-wave resonance with N given ones. Since any initial set of, say, M vectors can be complemented up to an isolated set of N modes by adding $N - M$ extra modes with zero initial amplitudes, there is no loss of generality. A wave field with a single non-zero amplitude $b(\boldsymbol{k}_0)$ corresponds to a Stokes wave, rather than a single Fourier harmonic in physical space; two non-zero amplitudes describe a short-crested wave, i.e. two oblique waves and a number of combination harmonics, etc. In this way, a modest number of $\boldsymbol{k}_j$ in the transformed space corresponds to a large number of physical-space harmonics. Say, for $O(\varepsilon^3)$ of the canonical transformation, $N = O(10^2)$ is approximately equivalent to $O(10^6)$ harmonics. In other words, numerical simulation within the framework of the Zakharov equation gives an enormous advantage from the viewpoint of computational resources required.

On the other hand, it is important to note that the procedure of discretization in the transformed space is not unique. In fact, the absence of limitations on the position of points $\boldsymbol{k}_j$ leads to the problem of finding objective methods of discretization. Any solution of the Zakharov equation corresponds, to within the accuracy of the given order of the canonical transformation, to a certain evolution of the wave field in terms of physical variables. It is essential that, at least in the conservative case, any exact solution of the discretized Zakharov equation coincides with the exact solution of the continuous equation with the same discrete initial conditions. However, the effect of discretization on the evolution of a given *continuous* amplitude spectrum is much more complicated than in the case of conventional physical-space models. The problem of the proper discretization of the Zakharov equation was recognized as an important challenge only very recently (Rasmussen & Stiassnie 1999), and so far little progress has been achieved. This problem remains a subject for further investigation. Fortunately, there are important physical situations where the choice of discretization is either evident for physical reasons (e.g. the case of a few well-pronounced interacting waves) or does not matter (e.g. the case of large wave ensembles where only statistical properties are important).

The present paper concentrates on the numerical study of the Zakharov equation itself, for problems where the initial conditions are formulated in terms of the complex amplitudes $b(\boldsymbol{k}_j)$. The paper is organized as follows. In the introductory § 2, the Hamiltonian formulation of surface wave dynamics is presented, and several most widely used computational techniques are briefly reviewed. Then, the derivation of the Zakharov equation is outlined, following the line of Krasitskii (1994), separately for capillary–gravity waves (taking account of three-wave processes), and for purely gravity waves (with four- and five-wave interactions included).

In § 3, the computational strategy for the Zakharov equation is discussed. First, an efficient Runge–Kutta-type algorithm is presented, for the general case of arbitrary $\boldsymbol{k}_j$, with the value of the timestep chosen to ensure the conservation of the known integrals with high accuracy (throughout the paper, the minimal accuracy of eight significant digits in the Hamiltonian is assumed). On the other hand, non-conservative effects, sufficiently small to preserve the Hamiltonian structure to the desired order, can also be included into the scheme. Then, a symplectic procedure for the integration of the purely conservative version of the equation is presented and discussed.

The rest of the paper provides examples of the application of the present method to three different problems. Each of these examples represents a problem of independent

scientific interest, and more complete results on some of them are published elsewhere. In the present article we provide a brief summary of the results in order to demonstrate the advantages of the proposed algorithm and, in particular, its application to problems where the use of other existing methods would have been difficult or impossible.

In § 4.1, in order to outline the inherent limitations of any numerical modelling of water waves and to address the problem of the predictability of the evolution of gravity and gravity–capillary waves, we consider the long-term evolution of wave systems with different (from relatively small to moderately large) numbers of interacting modes. The present method, being a very economical tool for the numerical simulations of such systems with the necessary control of accuracy, is also very convenient for studying the relative role of different types of interactions, due to its physical transparency.

In § 4.2, a simple model of three-dimensional sporadic crescent-shaped patterns on water surface is discussed, on the basis of the study of the evolution of a steep gravity wave embedded into wide-spectrum primordial noise and subjected to small non-conservative effects. In this example, the use of a conventional numerical technique would meet substantial difficulties in resolving the very narrow resonance zones and carrying out simulations for a large number of modes over $O(10^3)$ wave periods. By employing the proposed algorithm, the primary mechanism of the emergence of these patterns is revealed at little numerical cost.

In § 4.3, in order to demonstrate the performance of the present method for systems with a very large number of degrees of freedom, we consider the evolution of a single gravity wave with a large number of random satellites, thus modelling the evolution of a relatively steep wave immersed in a small-amplitude broad-band noise field. The simulation of the long-term evolution with the number of satellites taken (up to 10^3) requires only moderate computational resources; at the same time, this corresponds to millions of degrees of freedom in physical space.

2. Basic equations and the numerical model

2.1. *The Hamiltonian formulation*

We consider potential gravity waves on the free surface of a homogeneous, incompressible and inviscid fluid of infinite depth. The fluid is considered to be laterally unbounded, and the effects of atmospheric pressure are neglected. In terms of the coordinate system with origin located at the undisturbed water surface, with the vertical axis z oriented upward and the horizontal axes x, y, the governing equations have the form

$$\left.\begin{array}{l} \left.\begin{array}{l} \nabla^2\varphi = 0, \\ \varphi_t + gz + \frac{1}{2}(\nabla\varphi)^2 + \dfrac{p}{\rho} = 0, \end{array}\right\} \quad -\infty < z \leqslant \zeta(\boldsymbol{x}, t), \\ \lim\limits_{z\to-\infty} \varphi_z = 0, \\ \left.\begin{array}{l} \zeta_t + \nabla_x\varphi \cdot \nabla_x\zeta - \varphi_z = 0, \\ p = -\gamma\rho\nabla_x[\nabla_x\zeta(1 + (\nabla_x\zeta)^2)^{-1/2}], \end{array}\right\} \quad z = \zeta(\boldsymbol{x}, t), \end{array}\right\} \tag{2.1}$$

where $\nabla = (\partial/\partial x, \partial/\partial y, \partial/\partial z)$, $\nabla_x = (\partial/\partial x, \partial/\partial y)$, $\varphi(\boldsymbol{x}, z, t)$ is the velocity potential, γ is the coefficient of surface tension, p denotes pressure, ρ is the constant density of

the fluid, $z = \zeta(\boldsymbol{x}, t)$ specifies the free surface, $\boldsymbol{x} = (x, y)$ is a horizontal vector, t is time. It is convenient to define the surface potential

$$\psi(\boldsymbol{x}, t) = \varphi(\boldsymbol{x}, \zeta(\boldsymbol{x}, t), t),$$

then, as shown by Zakharov (1968), system (2.1) can be reformulated in terms of Hamilton equations in canonically conjugated variables ζ and ψ:

$$\frac{\partial \zeta(\boldsymbol{x}, t)}{\partial t} = \frac{\delta H}{\delta \psi(\boldsymbol{x}, t)}, \quad \frac{\partial \psi(\boldsymbol{x}, t)}{\partial t} = -\frac{\delta H}{\delta \zeta(\boldsymbol{x}, t)}, \tag{2.2}$$

where δ denotes the operator of functional differentiation, and the Hamiltonian H is the total energy of the system, namely

$$H = \frac{1}{2}\int_{-\infty}^{\zeta}\left[(\nabla\varphi)^2 + \left(\frac{\partial\varphi}{\partial z}\right)^2\right] \mathrm{d}z\,\mathrm{d}\boldsymbol{x} + \frac{1}{2}g\int \zeta^2\,\mathrm{d}\boldsymbol{x} + \gamma\int[\sqrt{1+(\nabla_x\zeta)^2}-1]\,\mathrm{d}\boldsymbol{x}, \tag{2.3}$$

where integration with respect to $\boldsymbol{x}$ over the entire horizontal plane is implied. In the domain $-\infty < z < \zeta(\boldsymbol{x}, t)$ for all $\boldsymbol{x}$, the Laplace equation

$$\nabla^2\varphi = 0 \tag{2.4}$$

must be satisfied; at the same time, the kinematic and dynamic boundary conditions are included in (2.2), (2.3). In order to get a closed system in ψ, ζ, one has to calculate H in terms of these variables, that is, to solve the boundary value problem

$$\nabla^2\varphi = 0,$$

$$\varphi(\boldsymbol{x}, \zeta) = \psi,$$

$$\varphi_z(\boldsymbol{x}, z) \to 0 \quad \text{as} \quad z \to -\infty.$$

An approximate solution can be obtained by performing the expansion in the parameter $k\zeta$ in the Hamiltonian, assuming that $k\zeta = O(\varepsilon) \ll 1$. Making the Fourier transformation

$$\zeta(\boldsymbol{x}) = \frac{1}{2\pi}\int \zeta(\boldsymbol{k})\,\mathrm{e}^{\mathrm{i}\boldsymbol{k}\boldsymbol{x}}\,\mathrm{d}\boldsymbol{k}, \quad \psi(\boldsymbol{x}) = \frac{1}{2\pi}\int \psi(\boldsymbol{k})\,\mathrm{e}^{\mathrm{i}\boldsymbol{k}\boldsymbol{x}}\,\mathrm{d}\boldsymbol{k}, \tag{2.5}$$

where integration is performed over the entire $\boldsymbol{k}$-plane, $\boldsymbol{k} = (k_x, k_y)$, and introducing complex variables $a(\boldsymbol{k})$,

$$\zeta(\boldsymbol{k}) = M(\boldsymbol{k})[a(\boldsymbol{k}) + a^*(-\boldsymbol{k})], \quad \psi(\boldsymbol{k}) = -\mathrm{i}N(\boldsymbol{k})[a(\boldsymbol{k}) - a^*(-\boldsymbol{k})], \tag{2.6}$$

$$M(\boldsymbol{k}) = \left[\frac{q(\boldsymbol{k})}{2\omega(\boldsymbol{k})}\right]^{1/2}, \quad N(\boldsymbol{k}) = \left[\frac{\omega(\boldsymbol{k})}{2q(\boldsymbol{k})}\right]^{1/2},$$

equations (2.2) take the form

$$\mathrm{i}\frac{\partial a(\boldsymbol{k})}{\partial t} = \frac{\delta H}{\delta a^*(\boldsymbol{k})}, \tag{2.7}$$

where an asterisk means the complex conjugate, $\omega(\boldsymbol{k}) = [\tau(\boldsymbol{k})q(\boldsymbol{k})]^{1/2}$ is the linear dispersion relation, $\tau(\boldsymbol{k}) = g + \gamma|\boldsymbol{k}|^2$; for the case of infinite depth considered here, $q(\boldsymbol{k}) = |\boldsymbol{k}| = k$. Without the loss of generality, it is convenient to set the gravitational acceleration to unity, with the corresponding change of length scale. In (2.7), the Hamiltonian H is a functional of $a(\boldsymbol{k})$, $a^*(\boldsymbol{k})$, and, in the form of a series in powers

of these variables, in the generic case can be written as

$$
\begin{aligned}
H = &\int \omega_0 a_0^* a_0 \,\mathrm{d}\boldsymbol{k}_0 \\
&+ \int U^{(1)}_{012}(a_0^* a_1 a_2 + a_0 a_1^* a_2^*)\delta_{0-1-2}\,\mathrm{d}\boldsymbol{k}_{012} \\
&+ \frac{1}{3}\int U^{(3)}_{012}(a_0^* a_1^* a_2^* + a_0 a_1 a_2)\delta_{0+1+2}\,\mathrm{d}\boldsymbol{k}_{012} \\
&+ \int V^{(1)}_{0123}(a_0^* a_1 a_2 a_3 + a_0 a_1^* a_2^* a_3^*)\delta_{0-1-2-3}\,\mathrm{d}\boldsymbol{k}_{0123} \\
&+ \frac{1}{2}\int V^{(2)}_{0123} a_0^* a_1^* a_2 a_3 \delta_{0+1-2-3}\,\mathrm{d}\boldsymbol{k}_{0123} \\
&+ \frac{1}{4}\int V^{(4)}_{0123}(a_0^* a_1^* a_2^* a_3^* + a_0 a_1 a_2 a_3)\delta_{0+1+2+3}\,\mathrm{d}\boldsymbol{k}_{0123} \\
&+ \int W^{(1)}_{01234}(a_0^* a_1 a_2 a_3 a_4 + a_0 a_1^* a_2^* a_3^* a_4^*)\delta_{0-1-2-3-4}\,\mathrm{d}\boldsymbol{k}_{01234} \\
&+ \frac{1}{2}\int W^{(2)}_{01234}(a_0^* a_1^* a_2 a_3 a_4 + a_0 a_1 a_2^* a_3^* a_4^*)\delta_{0+1-2-3-4}\,\mathrm{d}\boldsymbol{k}_{01234} \\
&+ \frac{1}{5}\int W^{(5)}_{01234}(a_0^* a_1^* a_2^* a_3^* a_4^* + a_0 a_1 a_2 a_3 a_4)\delta_{0+1+2+3+4}\,\mathrm{d}\boldsymbol{k}_{01234} \\
&+ \cdots .
\end{aligned}
\tag{2.8}
$$

The real interaction coefficients $U^{(n)}$, $V^{(n)}$, $W^{(n)}$ are known functions of the wavenumbers $\boldsymbol{k}_j$ and frequencies ω_j, given in Krasitskii (1994). Following that article, we use here the compact notation, replacing the arguments $\boldsymbol{k}_j$ of all the corresponding functions by the subscripts j, assigning the subscript zero to $\boldsymbol{k}$. Thus, $a_j = a(\boldsymbol{k}_j, t)$, $\omega_j = \omega(\boldsymbol{k}_j)$, $U^{(n)}_{012} = U^{(n)}(\boldsymbol{k}_0, \boldsymbol{k}_1, \boldsymbol{k}_2)$, $\delta_{0-1-2} = \delta(\boldsymbol{k}_0 - \boldsymbol{k}_1 - \boldsymbol{k}_2)$, etc. In the same way, $\mathrm{d}k_0 = \mathrm{d}k$, $\mathrm{d}k_{012} = \mathrm{d}k_0\,\mathrm{d}k_1\,\mathrm{d}k_2$, etc., and the integration is again performed over the entire $\boldsymbol{k}$-plane.

The Hamiltonian (2.8), by virtue of (2.7), gives the evolution equation, up to the fifth order in ε, in the form

$$
\begin{aligned}
\mathrm{i}\frac{\partial a_0}{\partial t} = \frac{\delta H}{\delta a_0^*} &= \omega_0 a_0 + \int U^{(1)}_{012} a_1 a_2 \delta_{0-1-2}\,\mathrm{d}\boldsymbol{k}_{12} \\
&+ 2\int U^{(1)}_{210} a_1^* a_2 \delta_{0+1-2}\,\mathrm{d}\boldsymbol{k}_{12} + \int U^{(3)}_{012} a_1^* a_2^* \delta_{0+1+2}\,\mathrm{d}\boldsymbol{k}_{12} \\
&+ \int V^{(1)}_{0123} a_1 a_2 a_3 \delta_{0-1-2-3}\,\mathrm{d}\boldsymbol{k}_{123} + \int V^{(2)}_{0123} a_1^* a_2 a_3 \delta_{0+1-2-3}\,\mathrm{d}\boldsymbol{k}_{123} \\
&+ 3\int V^{(1)}_{3210} a_1^* a_2^* a_3 \delta_{0+1+2-3}\,\mathrm{d}\boldsymbol{k}_{123} + \int V^{(4)}_{0123} a_1^* a_2^* a_3^* \delta_{0+1+2+3}\,\mathrm{d}\boldsymbol{k}_{123} \\
&+ \int W^{(1)}_{01234} a_1 a_2 a_3 a_4 \delta_{0-1-2-3-4}\,\mathrm{d}\boldsymbol{k}_{1234} + \int W^{(2)}_{01234} a_1^* a_2 a_3 a_4 \delta_{0+1-2-3-4}\,\mathrm{d}\boldsymbol{k}_{1234} \\
&+ \frac{3}{2}\int W^{(2)}_{43210} a_1^* a_2^* a_3 a_4 \delta_{0+1+2-3-4}\,\mathrm{d}\boldsymbol{k}_{1234} \\
&+ 4\int W^{(1)}_{43210} a_1^* a_2^* a_3^* a_4 \delta_{0+1+2+3-4}\,\mathrm{d}\boldsymbol{k}_{1234} \\
&+ \int W^{(5)}_{01234} a_1^* a_2^* a_3^* a_4^* \delta_{0+1+2+3+4}\,\mathrm{d}\boldsymbol{k}_{1234}.
\end{aligned}
\tag{2.9}
$$

2.2. *Numerical applications*

The above mathematical formulation obtained by the expansion in powers of ε gives a number of possibilities for constructing an algorithm for the numerical simulations of a wave field.

The most straightforward and powerful approach would be the direct integration of the primitive equations, in the form (2.1) or similar, for example using the mixed Eulerian–Lagrangian scheme of Longuet-Higgins & Cokelet (1976). This *fully nonlinear* approach allows the study of waves of any steepness up to overturning. However, if only small and moderate steepnesses are to be considered, in many cases the approach turns out to be too expensive in computational resources, since in this case the explicit use of the steepness as a small parameter generally reduces the computational costs by about 1–2 orders of magnitude.

One of the most popular methods for the simulation of the evolution of three-dimensional wave fields is built on the basis of the boundary conditions on the free surface, obtained from (2.1) with the surface tension effects omitted and expressed in terms of ψ, ζ:

$$\left.\begin{aligned} &\zeta_t + \nabla_x\psi\cdot\nabla_x\zeta - (1+\nabla_x\zeta\cdot\nabla_x\zeta)\varphi_z(x,\zeta,t) = 0,\\ &\psi_t + \zeta + \tfrac{1}{2}\nabla_x\psi\cdot\nabla_x\psi - \tfrac{1}{2}(1+\nabla_x\zeta\cdot\nabla_x\zeta)\varphi_z^2(x,\zeta,t) = 0. \end{aligned}\right\} \tag{2.10}$$

Equations (2.10) must be complemented by Laplace's equation (2.4). The velocity potential $\varphi(\boldsymbol{x},z,t)$ is expanded in powers of ε as

$$\varphi(\boldsymbol{x},z,t) = \sum_{m=1}^{M}\varphi_m(\boldsymbol{x},z,t),$$

where φ_m is of the order of ε^m, up to a certain number M that is the specified order of approximation in nonlinearity (usually, $M = O(10)$). Then, each φ_m is further expanded in a Taylor series about $z = 0$, obtaining by substitution into (2.10) a sequence of Dirichlet problems for $\varphi_m(\boldsymbol{x},z)$ with simple boundary geometry. For numerical purposes, φ_m is expressed by a double discrete Fourier transform, obtaining a large number of free Fourier modes, $N = O(10^3)$, in each horizontal dimension. The resulting equations are solved using a pseudospectral method, using a fast Fourier transform to efficiently project between the wavenumber and physical spaces. This *high-order spectral method* is known in two variants (Dommermuth & Yue 1987; West *et al.* 1987), differing in the method of calculating the vertical velocity and in the way of removing the aliasing error. The former scheme appears to be more popular; however, as noted by Tanaka (2001), the latter is preferable since it fully retains the Hamiltonian structure of the original system.

Another numerical method is based on the evolution equation written in terms of the functions $\zeta(\boldsymbol{k})$ and $\psi(\boldsymbol{k})$, again up to $O(\varepsilon^5)$, as

$$\begin{aligned} \frac{\partial\zeta_0}{\partial t} - q_0\psi_0 = {}& 2\int E^{(3)}_{-0,1,2}\psi_1\zeta_2\delta_{0-1-2}\,\mathrm{d}\boldsymbol{k}_{12} + 2\int E^{(4)}_{-0,1,2,3}\psi_1\zeta_2\zeta_3\delta_{0-1-2-3}\,\mathrm{d}\boldsymbol{k}_{123}\\ &+2\int E^{(5)}_{-0,1,2,3,4}\psi_1\zeta_2\zeta_3\zeta_4\delta_{0-1-2-3-4}\,\mathrm{d}\boldsymbol{k}_{1234}, \end{aligned} \tag{2.11a}$$

$$\begin{aligned} \frac{\partial\psi_0}{\partial t} + \tau_0\zeta_0 = {}& -\int E^{(3)}_{1,2,-0}\psi_1\psi_2\delta_{0-1-2}\,\mathrm{d}\boldsymbol{k}_{12} - 2\int E^{(4)}_{1,2,3,-0}\psi_1\psi_2\zeta_3\delta_{0-1-2-3}\,\mathrm{d}\boldsymbol{k}_{123}\\ &-4\int \Pi^{(4)}_{1,2,3,-0}\zeta_1\zeta_2\zeta_3\delta_{0-1-2-3}\,\mathrm{d}\boldsymbol{k}_{123}\\ &-3\int E^{(5)}_{1,2,3,4,-0}\psi_1\psi_2\zeta_3\zeta_4\delta_{0-1-2-3-4}\,\mathrm{d}\boldsymbol{k}_{1234}, \end{aligned} \tag{2.11b}$$

where the coefficients $E^{(j)}$, $\Pi^{(4)}$ are given in Krasitskii (1994). The specific form of the coefficients $E^{(j)}$ allows the very efficient integration of system (2.11) rewritten in an operator form, using highly vectorized FFT routines (Pushkarev & Zakharov 1997). This may be termed the *convolution method*, since its high efficiency is based on the economical use of FFT for pseudo-spectral calculation of integrals of convolution type.

The main difficulty of both approaches is the nonlinear numerical instability, manifested in the growth of short-wave perturbations and usually attributed to small-scale breaking, observed in direct simulation (e.g. Longuet-Higgins & Cokelet 1976; Dold 1992). To suppress this instability, the use of non-physical damping terms is often required (Pushkarev & Zakharov 1997; Dold 1992).

An attempt to build a numerical scheme on the basis of the *non-reduced Zakharov equation* (2.9) was made by Tanaka (2001), who, however, noted the inefficiency of this algorithm due to the complexity of (2.9) and difficulties with its vectorization.

2.3. *The Zakharov equation*

Instead of direct application of the power of a vector computer to the Hamiltonian equations governing the physical-space variables, we will adopt a different strategy based on the specific properties of gravity and gravity–capillary surface waves. It is well-known (Zakharov 1968; Krasitskii 1994) that the numerous terms in the expansion (2.8) do not have equal significance; in each order m, only the processes satisfying the resonant conditions

$$\sum_{j=1}^{m} s_j \boldsymbol{k}_j = 0, \quad \sum_{j=1}^{m} s_j \omega_j = 0, \tag{2.12}$$

where $s_j = \pm 1$, are essential for the dynamics. If some combinations of signs s_j are prohibited by the dispersion relation, the corresponding terms can be removed from the expansion (2.8) by a special canonical transformation, allowing one to obtain the so-called 'effective Hamiltonian' (Zakharov 1968). For instance, for the capillary–gravity waves, in the leading order $m = 3$ the signs s_j cannot all be equal. For the case of gravity waves, considering the expansion up to ε^5, only two resonant processes are permitted:

$$k_1 + k_2 - k_3 - k_4 = 0, \quad \omega_1 + \omega_2 - \omega_3 - \omega_4 = 0, \tag{2.13}$$

and

$$k_1 + k_2 - k_3 - k_4 - k_5 = 0, \quad \omega_1 + \omega_2 - \omega_3 - \omega_4 - \omega_5 = 0. \tag{2.14}$$

Consider a canonical transformation from $a(\boldsymbol{k})$ to a new variable $b(\boldsymbol{k})$, postulating it in the form of integral-power series (Zakharov 1968; Krasitskii 1994)

$$\begin{aligned} a_0 = b_0 &+ \int A^{(1)}_{012} b_1 b_2 \delta_{0-1-2}\, \mathrm{d}\boldsymbol{k}_{12} \\ &+ \int A^{(2)}_{012} b_1^* b_2 \delta_{0+1-2}\, \mathrm{d}\boldsymbol{k}_{12} + \int A^{(3)}_{012} b_1^* b_2^* \delta_{0+1+2}\, \mathrm{d}\boldsymbol{k}_{12} \\ &+ \int B^{(1)}_{0123} b_1 b_2 b_3 \delta_{0-1-2-3}\, \mathrm{d}\boldsymbol{k}_{123} + \int B^{(2)}_{0123} b_1^* b_2 b_3 \delta_{0+1-2-3}\, \mathrm{d}\boldsymbol{k}_{123} \\ &+ \int B^{(3)}_{0123} b_1^* b_2^* b_3 \delta_{0+1+2-3}\, \mathrm{d}\boldsymbol{k}_{123} + \int B^{(4)}_{0123} b_1^* b_2^* b_3^* \delta_{0+1+2+3}\, \mathrm{d}\boldsymbol{k}_{123} \end{aligned}$$

$$+\int C^{(1)}_{01234} b_1 b_2 b_3 b_4 \delta_{0-1-2-3-4}\,\mathrm{d}\boldsymbol{k}_{1234} + \int C^{(2)}_{01234} b^*_1 b_2 b_3 b_4 \delta_{0+1-2-3-4}\,\mathrm{d}\boldsymbol{k}_{1234}$$
$$+\int C^{(3)}_{01234} b^*_1 b^*_2 b_3 b_4 \delta_{0+1+2-3-4}\,\mathrm{d}\boldsymbol{k}_{1234} + \int C^{(4)}_{01234} b^*_1 b^*_2 b^*_3 b_4 \delta_{0+1+2+3-4}\,\mathrm{d}\boldsymbol{k}_{1234}$$
$$+\int C^{(5)}_{01234} b^*_1 b^*_2 b^*_3 b^*_4 \delta_{0+1+2+3+4}\,\mathrm{d}\boldsymbol{k}_{1234} + \cdots. \tag{2.15}$$

The Hamiltonian system (2.7) under the transformation (2.15) has the form

$$\mathrm{i}\frac{\partial b(\boldsymbol{k})}{\partial t} = \frac{\delta \tilde{H}}{\delta b^*(\boldsymbol{k})}, \tag{2.16}$$

where $\tilde{H} = \tilde{H}(b, b^*)$. The specific choice of the coefficients $A^{(n)}$, $B^{(n)}$, $C^{(n)}$ enables *reduction* of the Hamiltonian, in other words, the essential simplification of $\tilde{H}$, which now contains resonant terms only. For the case of capillary–gravity waves, this reduction leads to the Hamiltonian of the form, to the leading order

$$\tilde{H} = \int \omega_0 b_0 b^*_0\,\mathrm{d}\boldsymbol{k}_0 + \int U^{(1)}_{012}(b^*_0 b_1 b_2 + b_0 b^*_1 b^*_2)\delta_{0-1-2}\,\mathrm{d}\boldsymbol{k}_{12} \tag{2.17}$$

and the corresponding three-wave reduced equation is

$$\mathrm{i}\frac{\partial b_0}{\partial t} = \omega_0 b_0 + \int U^{(1)}_{012} b_1 b_2 \delta_{0-1-2}\,\mathrm{d}\boldsymbol{k}_{12} + 2\int U^{(1)}_{210} b^*_1 b_2 \delta_{0+1-2}\,\mathrm{d}\boldsymbol{k}_{12}. \tag{2.18}$$

Comparing (2.18) to the leading order of (2.9), one can see a certain simplification for capillary–gravity waves. Meanwhile, for purely gravity waves, the gain is much more dramatic. The reduced Hamiltonian has the form

$$\tilde{H} = \int \omega_0 b_0 b^*_0\,\mathrm{d}\boldsymbol{k}_0 + \frac{1}{2}\int \tilde{V}^{(2)}_{0123} b^*_0 b^*_1 b_2 b_3 \delta_{0+1-2-3}\,\mathrm{d}\boldsymbol{k}_{123}$$
$$+\frac{1}{2}\int \tilde{W}^{(2)}_{01234}(b^*_0 b^*_1 b_2 b_3 b_4 + b_0 b_1 b^*_2 b^*_3 b^*_4)\delta_{0+1-2-3-4}\,\mathrm{d}\boldsymbol{k}_{1234} + \ldots, \tag{2.19}$$

so that the corresponding reduced equation, to the fifth order in ε, is

$$\mathrm{i}\frac{\partial b_0}{\partial t} = \omega_0 b_0 + \int \tilde{V}^{(2)}_{0123} b^*_1 b_2 b_3 \delta_{0+1-2-3}\,\mathrm{d}\boldsymbol{k}_{123}$$
$$+\int \tilde{W}^{(2)}_{01234} b^*_1 b_2 b_3 b_4 \delta_{0+1-2-3-4}\,\mathrm{d}\boldsymbol{k}_{1234}$$
$$+\frac{3}{2}\int \tilde{W}^{(2)}_{43210} b^*_1 b^*_2 b_3 b_4 \delta_{0+1+2-3-4}\,\mathrm{d}\boldsymbol{k}_{1234} \tag{2.20}$$

Equation (2.20), being a generalization of the original result of Zakharov (1968) to the next order in ε, is known as the five-wave Zakharov equation for gravity waves. The interaction coefficients of the reduced equation $\tilde{V}^{(2)}$ and $\tilde{W}^{(2)}$ are known in terms of $U^{(n)}$, $V^{(2)}$ and $U^{(n)}$, $V^{(n)}$, $W^{(2)}$ respectively. The corresponding expressions can be found in Krasitskii (1994); earlier publications (e.g. Crawford, Saffman & Yuen 1980; Caponi *et al.* 1982; Yuen & Lake 1982) contain various misprints, due to the length of the formulas. It should also be noted that the original Zakharov derivation, as well as a number of subsequent reformulations, dealt with the non-Hamiltonian version of the equation. The Hamiltonian version was first suggested by Zakharov in his comments to the Russian edition of Yuen & Lake (1982) and later systematically rederived by Krasitskii (1994).

Formulas (2.18), (2.20) represent the two forms of the Zakharov integrodifferential equation. It is convenient to eliminate the rapid change of phase by change of variable:

$$b(\boldsymbol{k},t) = B(\boldsymbol{k},t)\exp[-\mathrm{i}\omega(\boldsymbol{k})t],$$

obtaining respectively

$$\mathrm{i}\frac{\partial B_0}{\partial t} = \int U^{(1)}_{012} B_1 B_2\, \mathrm{e}^{\mathrm{i}(\omega_0-\omega_1-\omega_2)t}\,\delta_{0-1-2}\,\mathrm{d}\boldsymbol{k}_{12} + 2\int U^{(1)}_{210} B_1^* B_2\, \mathrm{e}^{\mathrm{i}(\omega_0+\omega_1-\omega_2)t}\,\delta_{0+1-2}\,\mathrm{d}\boldsymbol{k}_{12}. \tag{2.21}$$

and

$$\begin{aligned}\mathrm{i}\frac{\partial B_0}{\partial t} = {} & \int \tilde{V}^{(2)}_{0123} B_1^* B_2 B_3\, \mathrm{e}^{\mathrm{i}(\omega_0+\omega_1-\omega_2-\omega_3)t}\,\delta_{0+1-2-3}\,\mathrm{d}\boldsymbol{k}_{123} \\ & + \int \tilde{W}^{(2)}_{01234} B_1^* B_2 B_3 B_4\, \mathrm{e}^{\mathrm{i}(\omega_0+\omega_1-\omega_2-\omega_3-\omega_4)t}\,\delta_{0+1-2-3-4}\,\mathrm{d}\boldsymbol{k}_{1234} \\ & + \frac{3}{2}\int \tilde{W}^{(2)}_{43210} B_1^* B_2^* B_3 B_4\, \mathrm{e}^{\mathrm{i}(\omega_0+\omega_1+\omega_2-\omega_3-\omega_4)t}\,\delta_{0+1+2-3-4}\,\mathrm{d}\boldsymbol{k}_{1234}.\end{aligned} \tag{2.22}$$

The Zakharov equation in the form (2.21), (2.22) provides the basis for our subsequent numerical simulations. The specific ways performing wave modelling within the framework of this approach are discussed in the next section.

3. Numerical integration of the Zakharov equation

3.1. *Explicit Runge–Kutta algorithm*

In this section, we will discuss the procedure for the numerical integration of (2.22); (2.21) is treated analogously.

Suppose first, for simplicity, that an initial state of the fluid is given via a set of discrete complex amplitudes in the *transformed* space, i.e. $b_m \equiv b(\boldsymbol{k}_m)$, $m = 1, 2, \ldots, N$. The set of N modes is assumed to be *isolated* with respect to four- and five-wave resonances, in the sense that there are no harmonics that are in four- or five-wave resonance with N given ones. In order to clarify this point, consider three given harmonics with wavevectors $\boldsymbol{k}_1$, $\boldsymbol{k}_2$, $\boldsymbol{k}_3$ and frequencies ω_1, ω_2, ω_3. If the set of equations

$$\boldsymbol{K} = \sum_1^3 s_j \boldsymbol{k}_j, \quad \omega(\boldsymbol{K}) = \sum_1^3 s_j \omega_j + O(\varepsilon^2), \tag{3.1}$$

where $s_j = \pm 1$, is satisfied for a certain $\boldsymbol{K}$, then the mode with wavevector $\boldsymbol{K}$ and zero initial amplitude will grow, provided that all three harmonics $\boldsymbol{k}_j$, $j = 1, 2, 3$ have non-zero amplitudes. Consequently, the set of initial conditions must be extended to include the mode $\boldsymbol{K}$. Our initial set then comprises the three non-zero-amplitude modes $\boldsymbol{k}_1$, $\boldsymbol{k}_2$, $\boldsymbol{k}_3$ and a number m of zero-amplitude modes $\boldsymbol{K}_{(i)}$, where $i = 1, ..., m$, and m being the number of different solutions to (3.1). Similarly the procedure can be carried out for any given number of initially non-zero modes both for quartet and quintet interactions. The advantage of dealing with isolated systems is twofold. First, they represent exact solutions to the continuous Zakharov equation with discrete initial conditions; second, the fact that we know *a priori* the interacting modes for all times enables us to optimize significantly the numerical procedure that is discussed below.

As the first step, all the coefficients $\tilde{V}$ and $\tilde{W}$ are calculated by a preprocessing routine. The coefficients are sparse matrices, with a number of symmetry properties

(Krasitskii 1994). For efficiency they are stored in the form of long arrays, together with the indices of the corresponding amplitudes. Note that for N harmonics in the transformed space, the number of four-wave coefficients C_V is specified by the number of quadrangles built on N given oriented edges, satisfying the inequality

$$C_V \geqslant N(N+1)/2; \tag{3.2}$$

this is due to the fact that the system always possesses *trivial* resonances of the form $\tilde{V}_{mnmn}$, $1 \leqslant m,n \leqslant N$, representing nonlinear frequency shifts (Annenkov & Shrira 1999). In a generic case of a non-regular grid in the transformed space, the total number of four-wave coefficients remains $O(N^2)$. The number of five-wave coefficients is not limited from below and for most cases is far less than the number of four-wave ones (although this is again not true for regular grids).

For the subsequent integration in time, the discretized version of (2.22) is used,

$$\begin{aligned}
\mathrm{i}\frac{\partial B_m}{\partial t} = {} & \mathrm{i}\Gamma_m B_m + \sum_{n=1}^{N}\sum_{p=1}^{N}\sum_{q=1}^{N} \tilde{V}_{mnpq} B_n^* B_p B_q \, \mathrm{e}^{\mathrm{i}(\omega_m+\omega_n-\omega_p-\omega_q)t} \, \Delta_{m+n-p-q} \\
& + \sum_{n=1}^{N}\sum_{p=1}^{N}\sum_{q=1}^{N}\sum_{r=1}^{N} \tilde{W}_{mnpqr} B_n^* B_p B_q B_r \, \mathrm{e}^{\mathrm{i}(\omega_m+\omega_n-\omega_p-\omega_q-\omega_r)t} \, \Delta_{m+n-p-q-r} \\
& + \frac{3}{2}\sum_{n=1}^{N}\sum_{p=1}^{N}\sum_{q=1}^{N}\sum_{r=1}^{N} \tilde{W}_{rqpnm} B_n^* B_p^* B_q B_r \, \mathrm{e}^{\mathrm{i}(\omega_m+\omega_n+\omega_p-\omega_q-\omega_r)t} \, \Delta_{m+n+p-q-r},
\end{aligned} \tag{3.3}$$

where $m = 1, 2, \ldots, N$, Δ is the Kronecker symbol (Δ_m equals unity when $m = 0$ and zero otherwise). In a standard way to take into account weak non-conservative effects, terms of the form $\Gamma_m B_m$ are added to the right-hand side of the equation, with Γ_m sufficiently small to keep the Hamiltonian structure intact to a desired order. Say, the values of Γ_m for all m are allowed to be $O(\varepsilon^4)$ when quintet interactions are considered and $O(\varepsilon^3)$ or $O(\varepsilon^2)$ for the situations where the study is focused on quartet or triplet interactions, respectively.

Provided that all $\Gamma_m = 0$, equation (3.3) has the Hamiltonian of the form

$$\begin{aligned}
H = {} & \frac{1}{2}\sum_{m=1}^{N}\sum_{n=1}^{N}\sum_{p=1}^{N}\sum_{q=1}^{N} \tilde{V}^{(2)}_{mnpq} B_m^* B_n^* B_p B_q \, \mathrm{e}^{\mathrm{i}(\omega_m+\omega_n-\omega_p-\omega_q)t} \, \Delta_{m+n-p-q} \\
& + \frac{1}{2}\sum_{m=1}^{N}\sum_{n=1}^{N}\sum_{p=1}^{N}\sum_{q=1}^{N}\sum_{r=1}^{N} \tilde{W}^{(2)}_{mnpqr} (B_m^* B_n^* B_p B_q B_r + B_m B_n B_p^* B_q^* B_r^*) \\
& \times \mathrm{e}^{\mathrm{i}(\omega_m+\omega_n-\omega_p-\omega_q-\omega_r)t} \, \Delta_{m+n-p-q-r};
\end{aligned} \tag{3.4}$$

other motion integrals are the two components of momentum

$$I = \sum_{m=1}^{N} \boldsymbol{k}_m B_m B_m^*.$$

If the five-wave processes are absent (i.e. all $\tilde{W}^{(2)} \equiv 0$), then the action

$$A = \sum_{m=1}^{N} B_m B_m^*$$

is also conserved.

The standard fourth-order constant-step explicit Runge-Kutta algorithm is sufficient for most applications. Evidently, the computational cost for a direct calculation of sums on the right-hand side of (3.3) would be very large (proportional to N^4). In the proposed algorithm, this calculation is performed using the results of the preprocessing, by the componentwise multiplication of real arrays containing the values of coefficients and complex arrays containing the amplitudes B_m. Note that from the viewpoint of linear algebra, this operation is in fact the multiplication of a diagonal matrix and a vector and is easily vectorized. The number of operations required for the computation of four- and five-wave parts of (3.3) is of the order of the number of four- and five-wave coefficients respectively. This means that, according to (3.2), the operation count per timestep for a generic case is $O(N^2)$. However, it is important to bear in mind that N stands for the number of harmonics in the transformed space, corresponding to a much larger number of physical-space harmonics N_P. In the generic case, for the third-order canonical transformation, $N_P = O(N^3)$ (see examples below).

3.2. *Symplectic procedure*

The Zakharov equation (2.22), as well as its discretized counterpart (3.3) in the conservative case (i.e. $\Gamma_m \equiv 0$ for all m), is Hamiltonian, and now it is understood well that the explicit Runge–Kutta method described in the previous paragraph gives an approximation to the solution of the discretized equations that does not retain the fundamental symmetry properties of the exact solution and hence, in a sense, is valid for a relatively short time only (West 1992). The reason for this is the neglect of important special features of the dynamics of Hamiltonian systems, in particular the symplecticness of the solution operator (Sanz-Serna & Calvo 1994). As a result, standard integration techniques can only be applied for a limited time. Certainly, the question of whether this time is too short for phenomena studied depends on the problem; nevertheless, even while integrating for a relatively short time, it is often desirable to retain as much structure as possible (Cane, Marsden & Ortiz 1999).

The problem of building a symplectic algorithm for the Zakharov equation that would be theoretically optimal as well as numerically competitive goes beyond the scope of the present study. Instead, here we will use a general algorithm, derived from a generating function, for comparison with the conventional technique.

Following Channel & Scovel (1990), it is convenient to use a generating function of the third kind, $K(B_0^*, B)$,

$$B_0 = -\frac{\partial K}{\partial B_0^*}, \quad B^* = -\frac{\partial K}{\partial B}, \tag{3.5}$$

expanding it in timestep δ as

$$K = \sum_{m=0}^{\infty} \frac{\delta^m}{m!} K_m(B_0^*, B),$$

so that

$$B = B_0 + \sum_{m=1}^{\infty} \frac{\delta^m}{m!} B_m,$$

where

$$B_m = -\left(\frac{\partial K_m}{\partial B}\right)^*.$$

Then, using the equations of motion for B in the form (3.3), one can obtain, up to the fourth order (see Channel & Scovel 1990 for details),

$$K_1 = -\mathrm{i}H, \tag{3.6a}$$

$$K_2 = -\mathrm{i}\frac{\partial H}{\partial t} + \mathrm{i}\frac{\partial K_1}{\partial B}\frac{\partial H}{\partial B^*}, \tag{3.6b}$$

$$K_3 = -\mathrm{i}\frac{\partial^2 H}{\partial t^2} + 2\mathrm{i}\frac{\partial K_1}{\partial B}\frac{\partial^2 H}{\partial B^* \partial t} + \mathrm{i}\frac{\partial K_2}{\partial B}\frac{\partial H}{\partial B^*} - \mathrm{i}\sum_p\sum_q \frac{\partial K_1}{\partial B_p}\frac{\partial K_1}{\partial B_q}\frac{\partial^2 H}{\partial B_p^* \partial B_q^*}, \tag{3.6c}$$

$$\begin{aligned} K_4 = {} & -\mathrm{i}\frac{\partial^3 H}{\partial t^3} + 3\mathrm{i}\frac{\partial K_1}{\partial B}\frac{\partial^3 H}{\partial B^* \partial t^2} - 3\mathrm{i}\sum_p\sum_q \frac{\partial K_1}{\partial B_p}\frac{\partial K_1}{\partial B_q}\frac{\partial^3 H}{\partial B_p^* \partial B_q^* \partial t} \\ & + \mathrm{i}\frac{\partial K_3}{\partial B}\frac{\partial H}{\partial B^*} - 3\mathrm{i}\sum_p\sum_q \frac{\partial K_1}{\partial B_p}\frac{\partial K_2}{\partial B_q}\frac{\partial^2 H}{\partial B_p^* \partial B_q^*} \\ & + \mathrm{i}\sum_n\sum_p\sum_q \frac{\partial K_1}{\partial B_n}\frac{\partial K_1}{\partial B_p}\frac{\partial K_1}{\partial B_q}\frac{\partial^3 H}{\partial B_n^* \partial B_p^* \partial B_q^*}. \end{aligned} \tag{3.6d}$$

Here, H is the Hamiltonian of the form (3.4), with its explicit dependence on time taken into account.

These expressions are used to evaluate K to a desired order. Then the algorithm is formed on the basis of the pair of equations (3.5), rewritten as

$$B = B_0 + \sum_{m=0}^{\infty} \frac{\delta^m}{m!}\frac{\partial K_m}{\partial B_0^*}, \quad B^* = B_0^* - \sum_{m=0}^{\infty} \frac{\delta^m}{m!}\frac{\partial K_m}{\partial B}. \tag{3.7}$$

Formulae $\partial K_m(B_0^*, B)/\partial B$ and $\partial K_m(B_0^*, B)/\partial B_0^*$ for the Hamiltonian (3.4) and $m = 1, 2, 3$ are given in the Appendix. System (3.7), complemented by the condition of conjugacy of B and B^*, is overdetermined. Solution is obtained by iterations; it is useful to take the Runge–Kutta solution as the first guess.

3.3. *Error analysis*

Early attempts at the numerical analysis of the Zakharov equation used a model problem of Benjamin–Feir instability, consisting of a carrier and several pairs of initially small one-dimensional equally spaced satellites (Caponi *et al.* 1982; Yuen & Lake 1982; Krasitskii & Kalmykov 1993). In order to test the properties of the proposed algorithm, we choose a model example that is close in spirit. Consider the set of wavevectors consisting of a carrier $\boldsymbol{k}_0 = (1, 0)$ and 7 pairs of satellites, each pair satisfying the condition

$$2\boldsymbol{k}_0 = \boldsymbol{k}_j + \boldsymbol{k}_{j+1}, \quad j = 1, 2, \ldots, 7, \tag{3.8}$$

with irregular spacing (table 1), so that all the quartet interactions among the satellites have the form (3.8).

The initial amplitude of the carrier B_0 was taken to be unity (corresponding to steepness $\varepsilon \simeq 0.225$), the satellites had initial amplitudes equal to 0.014 and phases at $-\pi/4$. Integration was performed up to $\omega_0 T = 10^5$, where $\omega_0 = \omega(\boldsymbol{k}_0)$, by the Runge–Kutta algorithm and symplectic algorithms of various orders, with several values of timestep δ in the range $1/64 \leqslant \delta \leqslant 1$. Figure 1, where the dependence of amplitudes B_m on time up to $\omega_0 t = 5 \times 10^3$ is plotted, gives an idea of the initial stage of the evolution.

First, we numerically tested the order of the symplectic integration, with the results

j	$\boldsymbol{k}_j$	$\boldsymbol{k}_{j+1}$
1	(0.9014, 0)	(1.0986, 0)
2	(0.8075, 0)	(1.1925, 0)
3	(0.7021, 0)	(1.2979, 0)
4	(0.6011, 0)	(1.3989, 0)
5	(0.5085, 0)	(1.4915, 0)
6	(0.4012, 0)	(1.5988, 0)
7	(0.3020, 0)	(1.6980, 0)

TABLE 1. Position of satellites in the model of Benjamin–Feir instability.

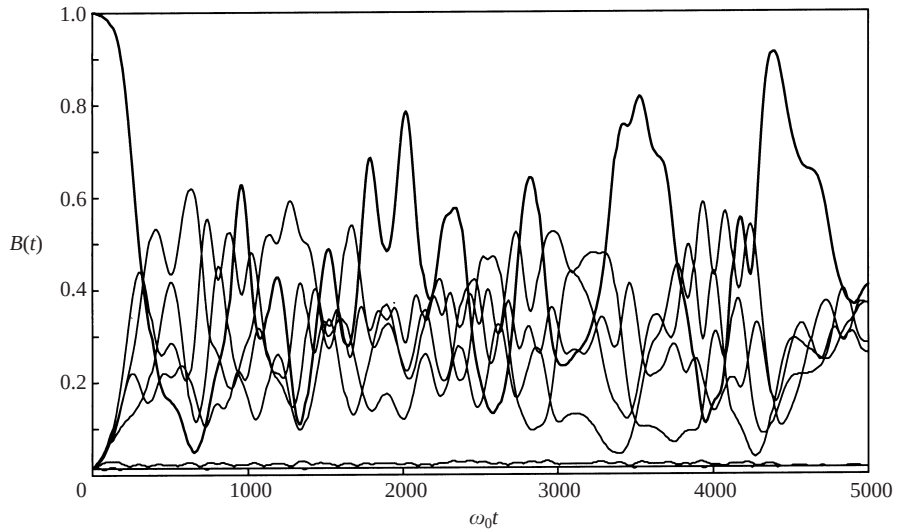

FIGURE 1. Evolution of the system comprising a carrier and 7 pairs of satellites (table 1). Dependence of mode amplitudes on time is shown.

shown in table 2. For the estimate of the error, we used the root-mean-square average of the deviation of energy from its starting value for all timesteps up to the fixed time $\omega_0 t = 10^3$. The respective orders of the algorithms are seen to be confirmed.

For a further check, we compared the dependence of energy conservation on time using the Runge–Kutta algorithm (RK) and symplectic integration of order 3 (SI3) for timesteps $\delta = 1/2$ and $1/4$. The results are shown in figure 2. While the energy error of RK increases monotonically with time, the error of SI3 oscillates about a certain value of energy, but does not show a secular growth in time. If the computation is continued for longer times, the growth of the RK error continues until the computation becomes meaningless, while the central value and amplitude of the energy oscillation for SI3 remain the same. Smaller timesteps considerably delay the time at which the RK error exceeds that of SI3, though the qualitative behaviour is similar. It appears that if a computation of the evolution is performed for a limited time, the RK algorithm with a smaller timestep can give better results, taking into account the efficiency of the explicit scheme. So far we have not come across a situation where the advantages of employing the symplectic algorithm outweigh the simplicity and efficiency of the RK algorithm, although we expect that such situations might occur.

We will demonstrate below that despite the superior energy conservation properties of the symplectic algorithm, the eventual chaotization of the system leads anyway to

	RK		SI2		SI3		SI4	
δ_n	ϵ_n	$\frac{\epsilon_{n-1}}{\epsilon_n}$	ϵ_n	$\frac{\epsilon_{n-1}}{\epsilon_n}$	ϵ_n	$\frac{\epsilon_{n-1}}{\epsilon_n}$	ϵ_n	$\frac{\epsilon_{n-1}}{\epsilon_n}$
0.5	2.4×10^{-9}	—	4.6×10^{-6}	—	6.3×10^{-9}	—	—	—
0.25	1.7×10^{-10}	14.4	1.1×10^{-6}	4.0	7.2×10^{-10}	8.7	4.6×10^{-10}	—
0.125	1.1×10^{-11}	15.2	2.8×10^{-7}	4.0	8.9×10^{-11}	8.2	2.9×10^{-11}	16.0
0.0625	6.9×10^{-13}	15.6	8.0×10^{-8}	4.0	1.1×10^{-11}	8.0	1.8×10^{-12}	16.0

TABLE 2. Error scaling for the value of the Hamiltonian as timestep δ is successively halved for the model of one-dimensional Benjamin–Feir instability using the explicit Runge–Kutta algorithm (RK) and symplectic integration of orders 2, 3 and 4 (SI2, SI3 and SI4 respectively). Error ϵ is calculated as the r.m.s. deviation of the Hamiltonian from its starting value to $\omega_0 t = 10^3$. The ratio of successive errors, close to the corresponding constant, confirms the order of the algorithms.

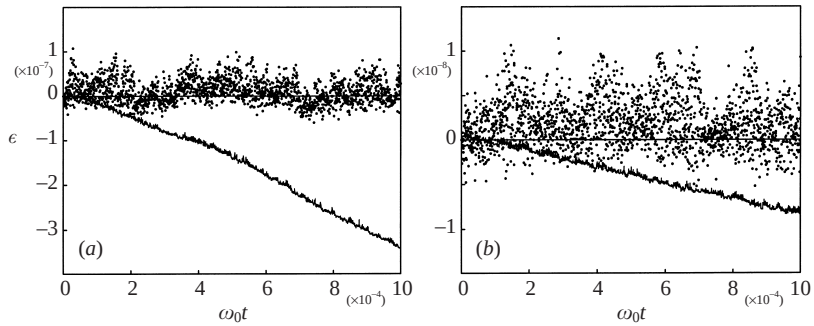

FIGURE 2. Comparison of energy error ϵ of a third-order symplectic algorithm (dotted curve) and a fourth-order Runge–Kutta algorithm (solid curve). The timestep is (*a*) 0.5 and (*b*) 0.25, equal for both methods.

the rapid loss of accuracy for the positions of *individual* trajectories and this loss does not depend on the integrator.

4. Examples

In order to illustrate the properties of the present method, we consider here three different examples of numerical applications. In these examples, we concentrate mainly on the numerical side of the corresponding problems, with only brief remarks on the physical aspects of the phenomena (which are discussed in more detail elsewhere).

First, we use the method for the study of the long-term evolution of the several low-dimensional consevative systems of gravity and gravity–capillary waves, with various numbers of interacting modes and different structures of interactions between them. For the case of gravity waves, a universal scenario of stochastization is demonstrated, and its quantitative characteristics are obtained. Second, the method is applied to the study of the formation of three-dimensional 'horseshoe' patterns on the water surface, often observed in laboratory experiments and in natural basins. A qualitative model of these patterns, explaining their sporadic nature, physical mechanisms of their selection and their specific asymmetric form, is suggested. The model is based on the simulation of a steep gravity wave embedded into wide-spectrum primordial noise and subjected to small non-conservative effects. Finally, to demonstrate the effectiveness of the method for multi-dimensional problems, we consider the long-time evolution of a Stokes wave immersed in noise field consisting of a very large number of degrees of freedom.

All examples are for infinitely deep water and in two horizontal dimensions. Note that in most cases, the long-term computations presented here cannot be performed with any other known method, since these methods would fail at some moment of time due to local steepening (and eventual overturning) of the water surface. In all computations, the standard fourth-order Runge–Kutta scheme was used, with timestep sufficiently small to ensure, in the conservative case, conservation of the integrals with high accuracy (at least 8 significant digits). Computations were performed on various computers, including AMD K6, AMD K7, Intel Pentium 2 processors and Silicon Graphics workstations, with typical times ranging from several minutes to several hours.

4.1. *Chaotization of gravity and gravity–capillary waves*

In our first set of numerical examples, we consider a number of nonlinear gravity and capillary wave systems from the viewpoint of their eventual chaotization. Although it is well-known that the phenomenon of chaotization is a general feature of non-integrable nonlinear systems, the quantitative characteristics of this process are unknown in many physical problems, in particular for surface waves. It is often assumed that the stochastization time scale significantly exceeds the characteristic times of the processes of interest. For instance, the evolution of water waves on time scales of the order of 10^2–10^3 characteristic wave periods is usually assumed to remain deterministic, and the field behaviour is considered as crucially depending on its initial configuration, i.e. the set of wavevectors and initial mode amplitudes (Yuen & Lake 1982). Hence, the unpredictability of evolution is often thought to be linked either to irreversible processes, or to numerical errors. In some recent numerical and experimental studies of gravity wave dynamics, difficulties in predictability of evolution were attributed to the existence of homoclinic structures in the exact equations (Ablowitz & Herbst 1990). However, this 'homoclinic chaos' disappears when discretization is sufficiently refined, or if an integrable difference scheme is employed.

Early computations (e.g. Caponi *et al.* 1982) showed that the solution for the initial configuration corresponding to a modulated periodic wavetrain manifests different regimes of evolution, including periodic and completely chaotic ones, depending on the degree of nonlinearity. However, only a limited and very specific choice of initial conditions was considered, without any attempt to find *quantitative* characteristics of chaotic behaviour.

In this section, we address the question of the limits of the deterministic approach in the water wave context by the numerical simulation of the evolution of a number of gravity- and capillary-gravity-wave systems, ranging from relatively simple (yet non-integrable) ones to complex wave ensembles with a large number of harmonics. The universality and physical transparency of the algorithm allows the quantitative characteristics of the stochastization process to be obtained and their dependence on various parameters studied, such as characteristic wave steepness, number of harmonics and structure of interactions. Only a few examples are presented; complete results are published in a separate article (Annenkov & Shrira 2001).

As the first non-trivial example, consider the simple non-integrable wave system comprising six harmonics lying on the same resonance curve, so that they form three resonant quartets

$$\left.\begin{aligned} \boldsymbol{k}_1 + \boldsymbol{k}_2 = \boldsymbol{k}_3 + \boldsymbol{k}_4 = \boldsymbol{k}_5 + \boldsymbol{k}_6, \\ \omega_1 + \omega_2 = \omega_3 + \omega_4 = \omega_5 + \omega_6. \end{aligned}\right\} \tag{4.1}$$

Harmonics $\boldsymbol{k}_{1-4}$ are fixed; in this example, they are chosen as $\boldsymbol{k}_1 = (1.0, 0.2)$, $\boldsymbol{k}_2 =$

$(1.2, -0.2)$, $\boldsymbol{k}_3 = (0.8, 0.27)$, $\boldsymbol{k}_4 = (1.4, -0.27)$. The remaining pair $\boldsymbol{k}_5 = (\kappa_1, \kappa_2)$, $\boldsymbol{k}_6 = (2.2 - \kappa_1, -\kappa_2)$ is moved along the resonance curve, where κ_1, the free parameter, satisfies the inequality $-0.29 < \kappa_1 < 1.05$ (figure 3*a*). Certainly, this gravity-wave infinite-depth model is invariant with respect to change of length scale, so that the choice $k = O(1)$ is a matter of convenience. Initial amplitudes $|B_m(0)|$ are calculated from the initial steepness ε of the interacting waves and randomly chosen initial phases θ_m,

$$B_m(0) = \pi \left(\frac{2\omega}{k_m}\right)^{1/2} \frac{\varepsilon}{k_m} \exp(\mathrm{i}\theta_m), \tag{4.2}$$

where $\varepsilon = 0.045$, 0.07 and 0.09 in separate runs. Then, this set of initial conditions is slightly perturbed to obtain the close set $\hat{B}_m(0)$, retaining the same values of the known integrals. The evolution of $B_m(t)$ and $\hat{B}_m(t)$, corresponding to two initially close trajectories of the same system, is traced up to $\omega t = 5 \times 10^5$.

In order to measure the divergence of phase trajectories of the system, the function

$$D(t) = \frac{\sum_m |B_m(t) - \hat{B}_m(t)|^2}{\sum_m |B_m(t)|^2} \tag{4.3}$$

is introduced, where the value of $D(0)$, obtained from $B_m(0)$ and the perturbed initial conditions $\hat{B}_m(0)$, is just above the roundoff error.

The evolution of D in the model (4.1) is shown in figure 3(*b*), for $\varepsilon = 0.07$ and different values of κ_1. If $\kappa_1 \leqslant -0.15$, the evolution is deterministic, with D growing only linearly with time. However, if $\kappa_1 > -0.15$, the initially close points diverge exponentially: $D(t)$ is approximately proportional to $\exp(\lambda t)$, where the value of λ can be estimated numerically. It is important to note that this divergence cannot be considered as a result of a phase shift between two simulations. The exponential growth of D continues until the distance between the trajectories becomes comparable to the size of the entire manifold. Since the value of D in (4.3) is normalized by wave action, it is limited by an $O(1)$ constant.

The normalized rate of divergence μ, where $\lambda = \mu\varepsilon^2\omega$, is shown in figure 3(*c*) as a function of κ_1, for three values of ε. The characteristic frequency ω is taken to be unity. In the outer part of the resonance curve (negative κ_1) the interaction is weak, and divergence is slow; however, above a certain critical value of κ_1 where the time dependence of D becomes clearly exponential, μ quickly reaches $O(1)$ and then varies rather slowly.

For a given value of κ_1, the value of λ must depend quadratically on wave steepness. This dependence was also verified numerically (Annenkov & Shrira 2001).

The system (4.1) comprises in fact three resonant quartet interactions. However, further experiments (Annenkov & Shrira 2001) show that for a given characteristic wave steepness (say, the largest steepness of interacting harmonics at the initial moment) the rate of divergence does not depend significantly on the number nor on the complexity of quartet interactions provided that non-integrability is ensured. Meanwhile, conditions of resonance in a nonlinear system need not be satisfied exactly. The increase of ε widens and shifts the resonance zones, effectively changing the number of active interactions in the system, so that the dependence of λ on ε^2 may deviate from direct proportionality. For instance, in Caponi *et al.* (1982) both increase and decrease of steepness made all satellites except for one pair leave the instability domain for the carrier, so that the evolution approached that of an integrable system.

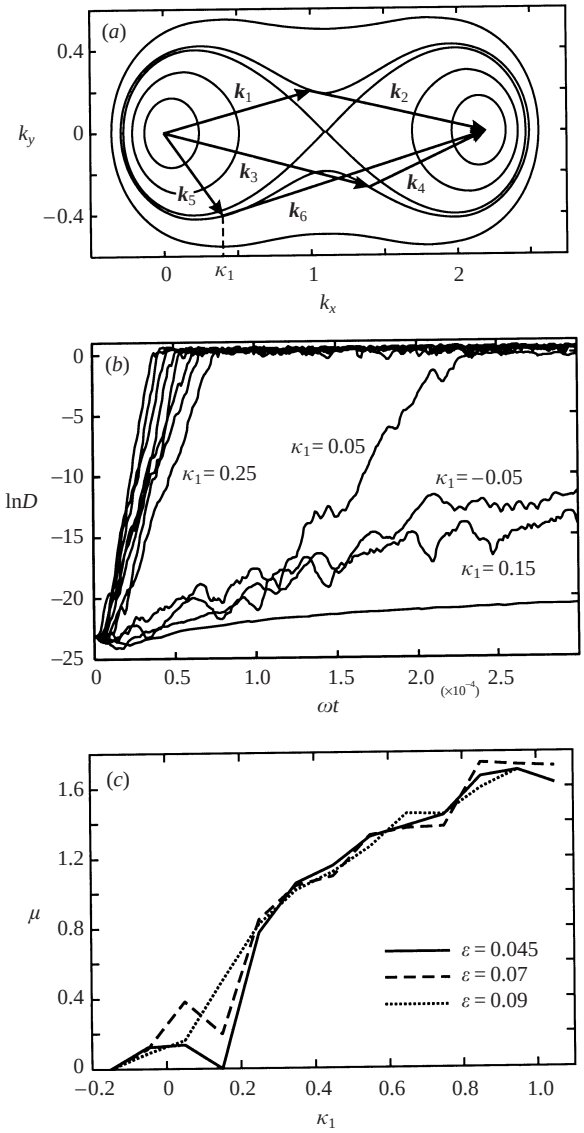

FIGURE 3. Divergence of phase trajectories in the system (4.1) of six waves forming three resonant quartets. (*a*) Position of wavevectors on the resonance curve. Vectors $\boldsymbol{k}_{1-4}$ are fixed; vectors $\boldsymbol{k}_5 = (\kappa_1, \kappa_2)$ and $\boldsymbol{k}_6$ are moved along the curve. (*b*) Divergence of phase trajectories for $\varepsilon = 0.07$ and different values of κ_1. (*c*) Normalized rate of divergence as function of κ_1, for three values of ε.

Another way to enrich the system (4.1) is to add pairs of five-wave satellites to each harmonic. However, numerical experiments (Annenkov & Shrira 2001) show that this also does not lead to considerable changes of μ.

In another example, consider the wave system in the form usual for studies of modulational instability, with the central harmonic $\boldsymbol{k}_0 = (1, 0)$ and N pairs $\boldsymbol{k}_j^{(1)}$, $\boldsymbol{k}_j^{(2)}$, so that

$$2\boldsymbol{k}_0 = \boldsymbol{k}_j^{(1)} + \boldsymbol{k}_j^{(2)}, \quad j = 1, 2, \ldots, N. \tag{4.4}$$

The pairs are chosen randomly in the domain $0 < \boldsymbol{k}_{jx} < 2$, $-0.4 < \boldsymbol{k}_{jy} < 0.4$. Initial amplitudes are all equal, again corresponding to three values of steepness $\varepsilon = 0.045$,

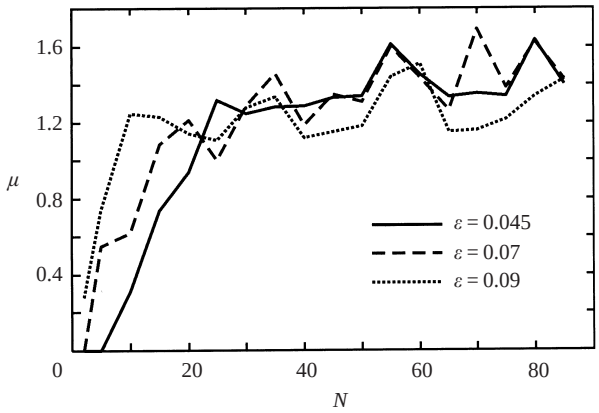

FIGURE 4. Dependence of the normalized divergence rate μ on the number of pairs of satellites in the model (4.4).

0.07 and 0.09; initial phases are random. The number N varies from 2 to 85. Note that in terms of physical variables $\varphi(\boldsymbol{k})$, $\eta(\boldsymbol{k})$ the case $N = 2$ corresponds to 43 Fourier harmonics in the physical space, while for $N = 85$ the number of harmonics exceeds 10^5.

The dependence of the value of μ on N is shown in figure 4. Since all the wavevectors $\boldsymbol{k}_j$ are chosen randomly, the increase in their number simply allows the harmonics to be placed at the points where they enter into more energetic interactions with the basic wave $\boldsymbol{k}_0$. Meanwhile, the same value of μ can be obtained for $N = 2$ (the simplest non-trivial case) by a special choice of harmonics.

Since the resonant interactions for capillary waves occur at the lowest order and therefore the characteristic interaction time is faster by a factor of $O(\varepsilon^{-1})$ than for gravity waves, it would be natural to expect the stochastization of capillary waves to occur faster by a factor of the same order.

However, numerical simulations (Annenkov & Shrira 2001) show that this is not the case: stochastization is much slower, in terms of characteristic time scale. Moreover, in contrast to gravity waves, the phenomenon of stochastization does not have a universal character: there is no characteristic value of the normalized exponent μ common for all systems sufficiently far from integrability. For a wave steepness of $O(10^{-1})$, the characteristic time scale of stochastization of a capillary-wave system has $O(10^3)$ wave periods, greatly exceeding the time scale of viscous dissipation. Besides that, the value of μ is sensitive to the number of linked triad interactions in the system, decreasing with the increase in the number of interactions.

The examples presented demonstrate that the stochastization of the gravity wave field, characterized by the exponential divergence of trajectories with the exponent remaining, in various models, close to $O(\varepsilon^2)$, is a generic phenomenon. The stochastization scenario is universal: the exponent does not show significant dependence on the number of modes nor on the number of interactions among them (provided that the model does not fall close to integrability). We stress that taking into account five-wave interactions does not alter the situation significantly and thus suggests the irrelevance of all the truncated higher-order terms in the Hamiltonian in the present context.

The characteristic time scale of the divergence is $O(\varepsilon^{-2})$. For the wave steepness of 0.1, typical of oceans and other natural basins, this means that the system tends to lose

all the information on the initial conditions over the time $\tau^* \simeq O(10^3)$ characteristic wave periods. In this sense, a deterministic way of describing water waves is essentially limited by this time scale, and the field evolution at time scales exceeding τ^* can be adequately described only within the framework of statistical models. This also implies that there is a 'grey area' where the statistical models resulting in the kinetic equation are not applicable yet, whereas a deterministic description is already invalid. The universality of the trajectories' instability and the exponents found enable one to estimate straightforwardly such statistical characteristics of the field as decorrelation time and the Sinai entropy.

A study of the long-term evolution of strictly conservative capillary–gravity waves is, of course, of mainly academic interest. However, the results of our simulations that contradict an intuitive expectation of faster stochastization of capillary waves, suggest the existence of an underlying peculiar mathematical structure. This phenomenon, as well as the reasons for fast and nearly universal stochastization of gravity waves, remain as challenging questions yet to be investigated.

4.2. *Formation of three-dimensional wave patterns*

The water surface in natural basins often manifests three-dimensional patterns of spectacular 'horseshoe' or 'crescent-shaped' form. These patterns, easily observed at early stages of wave development in the presence of a fresh wind, are characterized by the specific front–back asymmetry: front slopes are steeper than rear ones, and the convex sides of sharpened crests are always oriented downwind. Similar patterns were also observed in wave-tank experiments (e.g. Su *et al.* 1982; see Shrira, Badulin & Kharif 1996 for a list of references).

It has been established (first suggested by Su *et al.* 1982) that the inception mechanism of the horseshoes is due to McLean's class II instability (five-wave decay) of a plane basic wave. However, specific mechanisms of their formation were not identified.

In Shrira *et al.* (1996), a possible scenario of the emergence of the patterns was suggested, based on the assumption that the five-wave instability of a carrier may be considered as its interaction with the single symmetric pair with the largest linear growth rate. This (rather crude) assumption allowed the authors to consider the problem analytically, demonstrating the emergence of patterns with specific geometry closely resembling the observed horseshoes. The resemblance was due to *a special relation* between the phases of the interacting waves: the 'effective phase' $\theta = 3\alpha - 2\beta$, where α and β are the phases of the complex amplitude of the envelope of the basic wave and symmetric satellites respectively, must be negative, the best agreement with observations corresponding to the case $\theta = -\pi/2$. It was shown that non-conservative effects, inserted into the system but small enough to preserve the Hamiltonian structure to the required order, allow the system to evolve to a steady state with the geometric form of the free surface with the required characteristics.

However, although the domain of the five-wave instability is narrow, $O(\varepsilon^3)$ wide in the transverse direction, it is still a continuous finite size domain and there is no *a priori* reason to confine the consideration of this instability to a single pair of satellite harmonics. On the other hand, from the experimental viewpoint, the most often observed crescent-shaped patterns are *sporadic*. All this prompted us to look for a new robust mechanism able to create the essentially non-stationary, relatively short-lived patterns of the same geometry.

The first question to be addressed is the mechanism of the mode selection. Since in reality, a fundamental wave of a finite amplitude possesses finite size *domains*

of instability with respect to four- and five-wave processes in the wavevector space (see McLean 1982; Craik 1985, figure 6.6), simultaneous growth of a continuum of satellites should occur, which seems to be contrary to the observations. Although finite-size instability domains are common in many branches of applied mathematics, there is no way to approach such a problem analytically (Newell, Passot & Lega 1993). For a numerical simulation to succeed it has to overcome a number of obstacles. First, since the class II instability domains are narrow, $O(\varepsilon^3)$ wide, special care should be taken to ensure that the instability domain is well resolved, i.e. a large number of modes falls into the instability domain. Second, because the primary concern is the quintet interactions which occur on the background of much faster and stronger quartet interactions, the simulations should be carried out with very high accuracy over time spans of $O(\varepsilon^{-3})$. Given the sensitivity of the sporadic patterns at certain stages of their evolution to perturbations the task would be very challenging, unless the approach based on the Zakharov equation is employed.

We simulate the nonlinear dynamics of a continuum of linearly growing satellites by a sufficiently large number of unstable satellites. The 'sufficiency' is understood in the sense that adding more harmonics to the system does not alter the results and is checked *a posteriori*.

Thus, in our numerical study, we consider a system comprising a basic wave and a number of oblique (both symmetric, with respect to the k_x-axis, and non-symmetric) satellites, within and in the neighbourhood of the instability domain. The algorithm discussed in the present paper represents a perfect tool for such a simulation, since it gives the possibility of using an arbitrary number of satellites in arbitrary positions in Fourier space. Note that due to the fact that the five-wave resonance domains are narrow, the use of a conventional algorithm, with its restriction to regular grids, would necessitate extensive computational resources or would lead to unpredictable artefacts. Moreover, a moderate number of normal modes N found to be sufficient for simulations ($N = O(10^2)$) corresponds to N^4 modes in physical space, i.e. to $N_P = O(10^8)$, since in this case the fourth-order canonical transformation must be carried out. Furthermore, to study the three-dimensional processes *per se*, we have the flexibility to filter out the primarily two-dimensional modulational instability, choosing the initial satellites to be in the five-wave (class II) instability domain and stable part of the k-plane only, if we wish. This flexibility enables us, first, to develop an understanding of the main mechanisms of wave evolution due to quintet interactions only, and then to extend it to the general situation where more energetic quartet interactions coexist with the weaker but more important quintet interactions.

The problem of the formation of sporadic three-dimensional patterns was considered in detail in Annenkov & Shrira (1999); here, we will only outline the basic features of the evolution of a wave system comprising a carrier with wavevector $\boldsymbol{k}_0 = (1, 0)$ and N pairs of oblique satellites with wavevectors $\boldsymbol{k}_{j,j+1} = (\frac{3}{2} \pm p_j, \pm q_j)$, $j = 1, 2, \ldots, N$. For the satellites, conditions

$$\left.\begin{array}{ll} p_j = 0, & 1 \leqslant j \leqslant \frac{1}{2}N, \\ 1 < p_j < 2, \quad p_j \neq 0, & \frac{1}{2}N < j \leqslant N, \\ 1.48 \leqslant q_j \leqslant 1.68 & 1 \leqslant j \leqslant N, \end{array}\right\} \tag{4.5}$$

were imposed; in the experiments discussed here, $N = 42$, and the initial steepness of the fundamental is equal to 0.17. The satellites were set initially small, with the amplitudes of $O(10^{-2})$ relative to the amplitude of the fundamental; no significant dependence on the exact value of the satellites initial amplitude was revealed. For

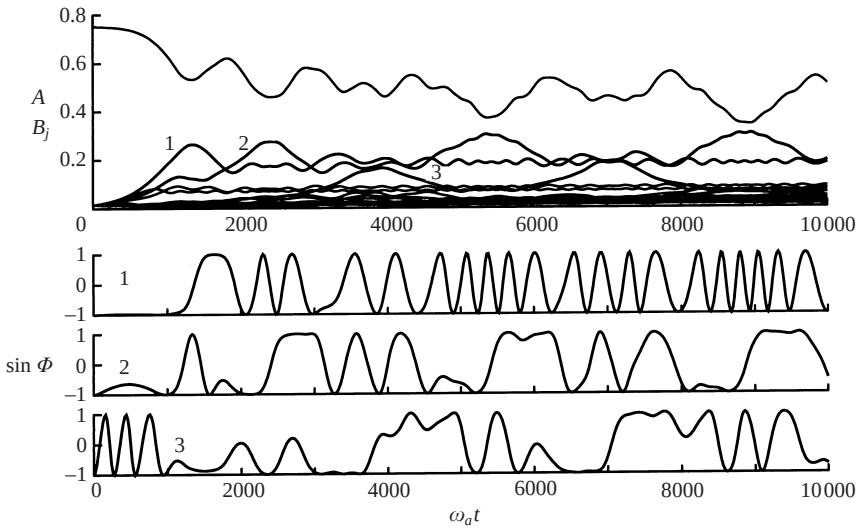

FIGURE 5. Evolution of the system of 85 waves obtained by numerical integration of the conservative Zakharov equation. The system consists of the basic wave, with initial amplitude $A(0) = 0.755$ (corresponding to steepness 0.17), and 42 pairs of initially small ($B_j(0) = 0.014$, $j = 1, 2, \ldots, 84$) satellites, chosen randomly in the $\boldsymbol{k}$-plane according to condition (4.5). For three most unstable pairs (numbered 1, 2, 3 in the amplitude plot), evolution of the 'effective phase' Φ, defined by (4.6), is shown.

each pair of satellites, the variable Φ (the phase of the pair of satellites relative to the fundamental, below referred to as 'the phase' for brevity) is defined as

$$\Phi = 3\alpha - \beta_1 - \beta_2, \tag{4.6}$$

where α, β_1, β_2 are the phases of the fundamental and two satellites respectively; initial values of Φ were prescribed at the value most favourable for growth ($-\pi/2$). Evolution in time was traced for about 10^3 periods of the basic wave. We emphasize that in these examples the Benjamin–Feir instability was excluded.

An example of the conservative evolution of the system is presented in figure 5. The plot demonstrates two distinct features of the class II instability with respect to multiple satellites. First, most of the modes located in the linear instability domain do not attain considerable amplitudes; instead, their growth is quickly arrested, resulting in stagnation at a quite low level. Only a few modes at each moment can grow unattenuated, though this behaviour is displayed by different modes at different moments. Second, the evolution of the phases of these growing modes differs noticeably from that of the isolated three-wave system. In particular, it becomes essentially asymmetric. While a mode is growing, its phase remains close to $-\pi/2$, as in the three-mode case; the maximum of the satellite amplitude again corresponds to zero phase, but soon after reaching the maximum of the amplitude, the phase typically starts to change much more rapidly, while the amplitude quickly decreases and tends to stagnate at a low level. It can be noticed, however, that the behaviour described is not always well pronounced for all growing pairs during the course of the *conservative* evolution, thus allowing one to consider it only as a tendency.

Meanwhile, in the more realistic weakly non-conservative case (figure 6), these features are much more pronounced. The phases of a few growing satellites are close to $-\pi/2$ during their growth and near the maximum, while during the decay

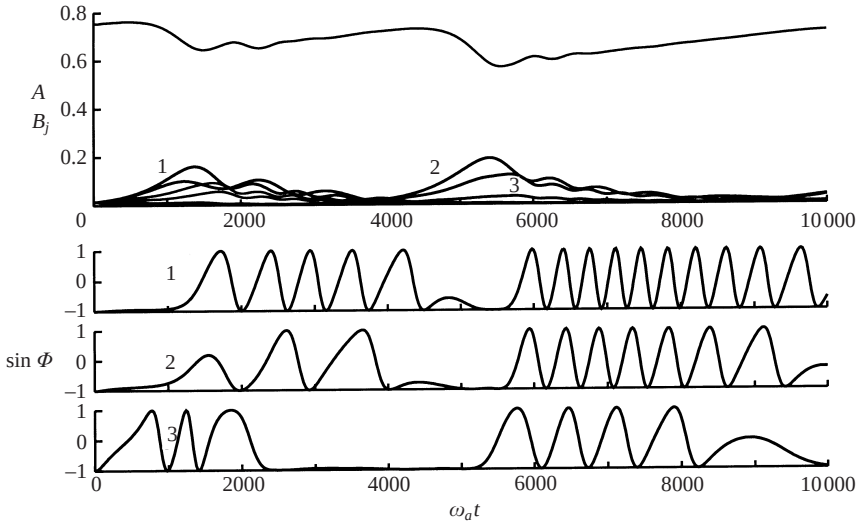

FIGURE 6. Evolution of the system of 85 harmonics obtained by integration of the Zakharov equation perturbed by small non-conservative effects. The system is the same as in figure 5, with weak forcing for the basic wave, $\Gamma_0 = 5 \times 10^{-5}\omega_0$, and weak dissipation for the satellites, $\Gamma_j = 5 \times 10^{-4}\omega_j$, $j = 1, 2, \ldots, N$, where Γ is the linear forcing/damping rate for each mode, introduced in (3.3).

the phases rapidly change. Taking into account Benjamin–Feir processes does not result in any qualitative changes of the evolution, although the time scale of the pattern formation increases (figure 7). Overall, the evolution of the satellites can be summarized as follows:

(i) at each particular moment *a maximum of one pair* is large, though at different moments different modes may prevail;

(ii) when a satellite pair starts to grow, its phase is set close to $-\pi/2$ and remains in this vicinity almost until the maximum of the satellite amplitude is reached; at the maximum of the amplitude the phase is still *negative*;

(iii) after the mode passes its point of maximum amplitude, the phase begins to change (rotate) rapidly;

(iv) if a satellite decays or does not grow, its phase rotates, passing quickly through all possible values.

These features of the behaviour were established in a large number of runs of the numerical model which required quite modest computational resources. On the basis of the simulations we briefly formulate the principal conclusions we arrived at in Annenkov & Shrira (1999). First, we found that the mode selection mechanism is due to the frequency detuning of the growing satellites caused by the quartet interactions: typically the mode with the largest amplitude 'pushes out' all other satellites from the resonance zone, thus stopping their growth at a quite low level (their amplitudes remain $O(\varepsilon^{1/2})$). Second, we revealed the sensitivity of the system at the stage of selection: a small perturbation can result in another pair of satellites dominating over a given cycle. Finally, we showed that the particular values of the phase between the central wave and the most developed satellites tend to prevail most of the time regardless of the initial conditions. Thus we were able to explain the basic features of the sporadic pattern phenomenology.

However, in a more general context, other aspects of the simulations are worth noting. It is commonly believed that in the process of water-wave nonlinear evolution

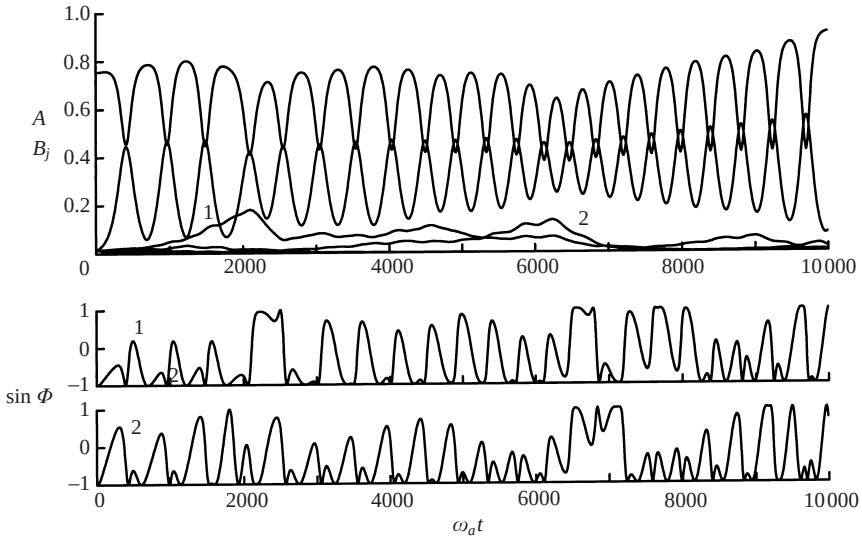

FIGURE 7. Evolution of the system of 87 harmonics obtained by integration of the Zakharov equation perturbed by small non-conservative effects. The system consists of the basic wave, with initial amplitude $A(0) = 0.755$ (corresponding to steepness 0.17), 42 pairs of initially small ($B_j(0) = 0.014$, $j = 1, 2, \ldots, 84$) five-wave satellites (the same set was used in figure 5), and one pair of four-wave (Benjamin–Feir) satellites ($\boldsymbol{k}_j = (1 \pm 0.27, 0)$), with the same initial amplitude. Weak forcing for the basic wave and weak dissipation for five-wave satellites ($\Gamma_0 = 5 \times 10^{-5}\omega_0$, $\Gamma_j = 5 \times 10^{-4}\omega_j$, $j = 1, 2, \ldots, N$) are included. For two most unstable five-wave pairs (numbered 1, 2 in the amplitude plot), evolution of phase is shown.

harmonics tend to multiply *ad infinitum* since the dissipation is very small. The plots in figures 6 and 7 show the opposite scenario of evolution: despite a large number of initial *unstable* modes, the dynamics of the wave field becomes effectively low-dimensional. Although the phenomenon is confined to a specific class of situations, we emphasize that it occurs primarily due to the effective nonlinear selection mechanism which is conservative in its nature. The presence of very small ($O(10^{-5})$) dissipation is also important but plays a secondary role.

4.3. *Evolution of a wave immersed in a noise field*

The primary aim of this example is to demonstrate the performance of the present method for problems with quite a large number of degrees of freedom. We consider a carrier with wavevector $\boldsymbol{k}_0 = (1, 0)$, relatively steep initially ($\varepsilon = 0.225$) and immersed in a field of noise, represented by N pairs of initially small satellites $\boldsymbol{k}_j^{(1)}$, $\boldsymbol{k}_j^{(2)}$, satisfying the condition

$$2\boldsymbol{k}_0 = \boldsymbol{k}_j^{(1)} + \boldsymbol{k}_j^{(2)}, \quad j = 1, 2, \ldots, N, \tag{4.7}$$

where the pairs are chosen randomly in the domain $0.2 < \boldsymbol{k}_{jx} < 1.8$, $-0.4 < \boldsymbol{k}_{jy} < 0.4$. In this example, $N = 500$, so that the system consists of 1001 harmonics overall.

Figure 8 shows the evolution of the system up to $\omega_0 t = 10^4$, where ω_0 is the carrier frequency ($\omega_0 = 1$). As the energy goes to satellites, the amplitude of the carrier (that initially accounts for more then 90% of the total energy of the ensemble) quickly decreases. At a certain value of time (600–800 periods of the carrier), the amplitudes of the central harmonic and of most unstable satellites attain values close to each other. Later, the carrier slightly oscillates, not exceeding 1–2% of the total energy. Note that, while this computation does not require much computational power (about

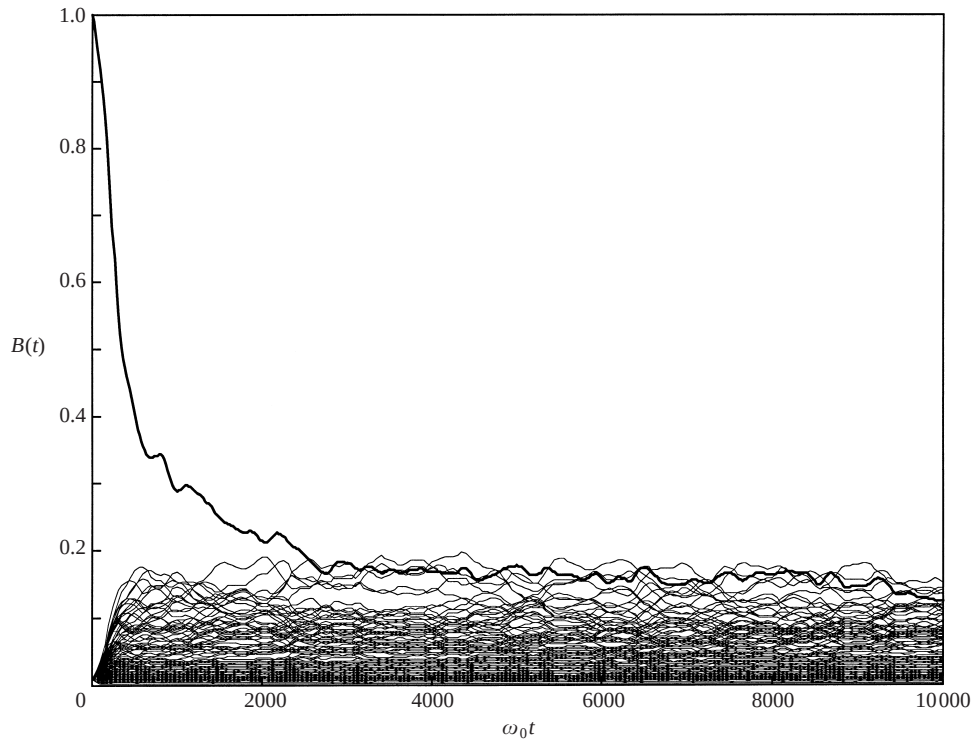

FIGURE 8. Evolution of a system consisting of a carrier, with the initial steepness 0.225, and 500 pairs of randomly chosen initially small oblique satellites, satisfying the condition (4.7). Evolution is shown up to $\omega_0 t = 10^4$, ω_0 being the frequency of the fundamental.

15 hours on a 800 MHz AMD K7 processor), in physical space the wave system under consideration corresponds to approximately 10^8 degrees of freedom, so that the computation of its long-term evolution with conventional numerical methods is impossible.

The distribution of energy in the $\boldsymbol{k}$-plane at $\omega_0 t = 5 \times 10^3$ is shown in figure 9. The unstable region is known to have the form of a pair of 'horseshoes' situated symmetrically with respect to the k_y-axis on both sides of the carrier (e.g. Crawford *et al.* 1981; Craik 1985). As might have been expected, we find that after the initial stage of the evolution where the dominant wave still far exceeds the noise, the energy is redistributed in this region, with small oscillations within it.

5. Discussion

In this paper we have considered an efficient and convenient method for the numerical study of water wave evolution, based on the reduced integrodifferential Zakharov equation. Owing to the enormous reduction in the number of interacting waves and wide separation of time scales, the algorithm allows numerical simulations for various physical problems to be performed, where the use of conventional algorithms would be difficult or impossible. It is important to note that a complete development of the method requires resolving the problem of discretization of the Zakharov equation. At present, this problem is unsolved, and its overcoming remains the key challenge for further progress.

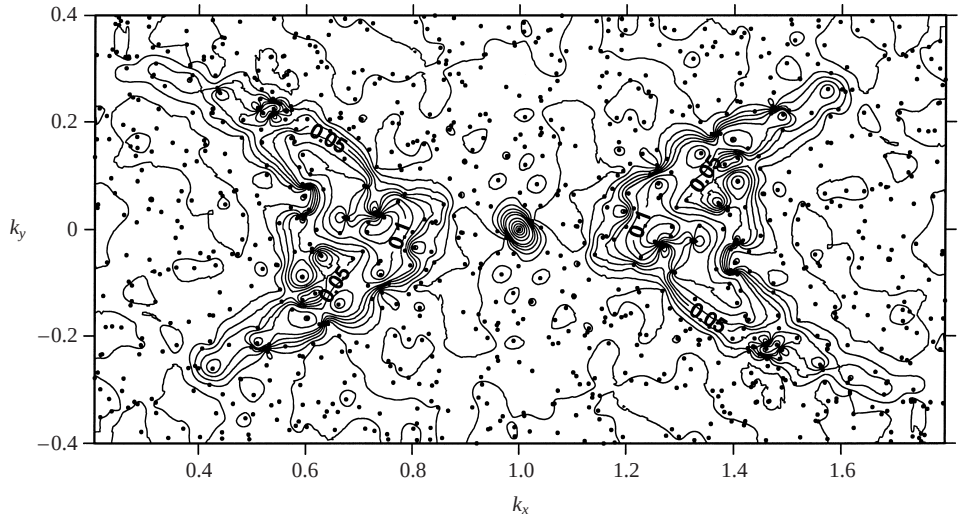

FIGURE 9. Distribution of wave amplitudes in Fourier space for the system shown in figure 8 at $\omega_0 t = 5 \times 10^3$. Points show positions of modes.

However, one can indicate a number of physical situations where the method can be effectively used in its present state. First, this refers to the case when a wave ensemle consists of a limited number of pronounced interacting modes. Investigation of various physical mechanisms responsible for the phenomena observed on a water surface often requires the numerical simulation of simple (although non-integrable) model problems. In this way, the present method, with its physical transparency, ability to manually prescribe different types of interactions, to switch on/off the higher-order processes and to use uneven grids for the better resolution of narrow resonance domains, is invaluable. In particular, the simulation of a number of models with a small and moderate number of interacting harmonics enabled us to find the important physical conclusion of unexpectedly fast stochastization of gravity waves and to make quantitative estimates of the stochastization time scale. On the other hand, the study of the instability of a carrier with respect to a number of oblique satellites allowed us to propose the physical mechanism for the emergence of sporadic horseshoe patterns on the surface, essential for the problems of remote sensing (Shrira, Badulin & Voronovich 2001).

Second, there are important physical situations where the problem of discretization is of a secondary importance, since the statistical properties of a wave ensemble are much more important than the choice of individual harmonics. There exists a well-established general formalism for treating the complex motion of a weakly nonlinear wave field (wave turbulence). The statistical description is provided by the kinetic equation for the second statistical moments of the field. The approach is based on the key hypothesis of quasi-Gaussianity of the statistically homogeneous wave field: the closure is made by assuming all odd statistical moments to be zero and expressing all higher-order even moments in terms of the second-order ones. Although the approach proved to be quite successful in addressing many experimental situations, the gap in its foundations due to the assumed quasi-Gaussianity of the field remains open. The range of validity of the kinetic equations remains yet to be specified. Moreover, recently the phenomenon of coherent patterns in wide-band random wave fields,

unexplainable within the classical kinetic framework, has been observed in many physical situations.

To our knowledge there have been no attempts to check the key quasi-Gaussianity hypothesis by direct numerical simulations. The difficulty lies in the fact that the primitive equations should be integrated for a very large number of modes over time intervals much larger than those required in simulations of strong turbulence. From this viewpoint, the present method provides a number of advantages, with the elimination of non-resonant modes and much faster integration of the equations. On the other hand, since the contributions of different terms to the Hamiltonian are much easier to trace, the method allows identification of the specific mechanisms leading to the departure of the field from quasi-Gaussianity and quantification of their contributions. This possibility to check the foundations of the existing statistical theory of water waves appears to be the most important direction for the future application of the method.

We are grateful to Dr M. Tanaka for valuable comments on the first draft of the manuscript. The work was supported by ONR under grant N00014-94-1-0532, by INTAS (grant 97-575), and by Russian Foundation for Basic Research (grant 01-05-64603).

Appendix. Formulae for symplectic integration

Expressions for the partial derivatives of the generating function $\partial K_j(B_0^*, B)/\partial B$ and $\partial K_j(B_0^*, B)/\partial B_0^*$, $j = 1, 2, 3$, have the form

$$\frac{\partial K_1(B_0^*, B)}{\partial B_{0m}^*} = -\mathrm{i}\frac{\partial H}{\partial B_{0m}^*}, \quad \frac{\partial K_1(B_0^*, B)}{\partial B_m} = -\mathrm{i}\frac{\partial H}{\partial B_m}, \tag{A 1a,b}$$

$$\frac{\partial K_2(B_0^*, B)}{\partial B_{0m}^*} = -\mathrm{i}\frac{\partial^2 H}{\partial B_{0m}^* \partial t} + \sum_j \left(\frac{\partial^2 H}{\partial B_{0m}^* \partial B_{0j}^*} \frac{\partial H}{\partial B_j} + \frac{\partial^2 H}{\partial B_{0m}^* \partial B_j} \frac{\partial H}{\partial B_{0j}^*} \right), \tag{A 2a}$$

$$\frac{\partial K_2(B_0^*, B)}{\partial B_m} = -\mathrm{i}\frac{\partial^2 H}{\partial B_m \partial t} + \sum_j \left(\frac{\partial^2 H}{\partial B_m \partial B_j} \frac{\partial H}{\partial B_{0j}^*} + \frac{\partial^2 H}{\partial B_m \partial B_{0j}^*} \frac{\partial H}{\partial B_j} \right), \tag{A 2b}$$

$$\begin{aligned}
\frac{\partial K_3(B_0^*, B)}{\partial B_{0m}^*} = &-\mathrm{i}\frac{\partial^3 H}{\partial B_{0m}^* \partial t^2} + \sum_j \left(\frac{\partial^2 H}{\partial B_{0m}^* \partial B_{0j}^*} \frac{\partial^2 H}{\partial B_j \partial t} + 2\frac{\partial^2 H}{\partial B_{0m}^* \partial B_j} \frac{\partial^2 H}{\partial B_{0j}^* \partial t} \right. \\
&\left. + \frac{\partial^3 H}{\partial B_{0m}^* \partial B_j \partial t} \frac{\partial H}{\partial B_{0j}^*} + 2\frac{\partial^3 H}{\partial B_{0m}^* \partial B_{0j}^* \partial t} \frac{\partial H}{\partial B_j} \right) \\
&-\mathrm{i}\sum_j \sum_k \left[\frac{\partial^3 H}{\partial B_{0m}^* \partial B_j \partial B_{0k}^*} \frac{\partial H}{\partial B_{0j}^*} \frac{\partial H}{\partial B_k} + \frac{\partial^3 H}{\partial B_{0m}^* \partial B_j \partial B_k} \frac{\partial H}{\partial B_{0j}^*} \frac{\partial H}{\partial B_{0k}^*} \right. \\
&+ \frac{\partial^2 H}{\partial B_{0m}^* \partial B_j} \left(\frac{\partial^2 H}{\partial B_{0j}^* \partial B_k} \frac{\partial H}{\partial B_{0k}^*} + 2\frac{\partial^2 H}{\partial B_{0j}^* \partial B_{0k}^*} \frac{\partial H}{\partial B_k} \right) \\
&\left. + \frac{\partial^2 H}{\partial B_{0m}^* \partial B_{0j}^*} \left(\frac{\partial^2 H}{\partial B_j \partial B_{0k}^*} \frac{\partial H}{\partial B_k} + 2\frac{\partial^2 H}{\partial B_j \partial B_k} \frac{\partial H}{\partial B_{0k}^*} \right) \right],
\end{aligned} \tag{A 3a}$$

$$\frac{\partial K_3(B_0^*,B)}{\partial B_m} = -\mathrm{i}\frac{\partial^3 H}{\partial B_m \partial t^2} + \sum_j \left(\frac{\partial^2 H}{\partial B_m \partial B_{0j}^*}\frac{\partial^2 H}{\partial B_j \partial t} + 2\frac{\partial^2 H}{\partial B_m \partial B_j}\frac{\partial^2 H}{\partial B_{0j}^* \partial t} + \frac{\partial^3 H}{\partial B_m \partial B_j \partial t}\frac{\partial H}{\partial B_{0j}^*} + 2\frac{\partial^3 H}{\partial B_m \partial B_{0j}^* \partial t}\frac{\partial H}{\partial B_j} \right)$$
$$-\mathrm{i}\sum_j \sum_k \left[\frac{\partial^3 H}{\partial B_m \partial B_{0j}^* \partial B_{0k}^*}\frac{\partial H}{\partial B_j}\frac{\partial H}{\partial B_k} + \frac{\partial^3 H}{\partial B_m \partial B_j \partial B_{0k}^*}\frac{\partial H}{\partial B_{0j}^*}\frac{\partial H}{\partial B_k} + \frac{\partial^2 H}{\partial B_m \partial B_j}\left(\frac{\partial^2 H}{\partial B_{0j}^* \partial B_k}\frac{\partial H}{\partial B_{0k}^*} + 2\frac{\partial^2 H}{\partial B_{0j}^* \partial B_{0k}^*}\frac{\partial H}{\partial B_k} \right) + \frac{\partial^2 H}{\partial B_m \partial B_{0j}^*}\left(\frac{\partial^2 H}{\partial B_j \partial B_{0k}^*}\frac{\partial H}{\partial B_k} + 2\frac{\partial^2 H}{\partial B_j \partial B_k}\frac{\partial H}{\partial B_{0k}^*} \right) \right]. \qquad (A\,3b)$$

These expressions are used for the numerical solution of (3.7) by iterations.

REFERENCES

Ablowitz, M. J. & Herbst, B. M. 1990 On homoclinic structure and numerically induced chaos for the nonlinear Schrödinger equation. *SIAM J. Appl. Maths* **50**, 339–351.

Annenkov, S. Yu. & Shrira, V. I. 1999 Sporadic wind wave horse-shoe patterns. *Nonlin. Proc. Geophys.* **6**, 27–50.

Annenkov, S. Yu. & Shrira, V. I. 2001 On the predictability of evolution of surface gravity and gravity-capillary waves. *Physica* D **152–153**, 665–675.

Cane, C., Marsden, J. E. & Ortiz, M. 1999 Symplectic-energy-momentum preserving variational integrators. *J. Math. Phys.* **40**, 3353–3371.

Caponi, E. A., Saffman, P. G. & Yuen, H. C. 1982 Instability and confined chaos in a nonlinear dispersive wave system. *Phys. Fluids* **25**, 2159–2166.

Chalikov, D. & Sheinin, D. 1996 Numerical modeling of surface waves based on principal equations of potential wave dynamics. *Tech. note*. NOAA/NWS/NCEP Ocean Modeling Branch.

Chalikov, D. & Sheinin, D. 1998 Direct modeling of one-dimensional nonlinear potential waves. In *Nonlinear Ocean Waves* (ed. W. Perrie). Advances in Fluid Mechanics, vol. 17, pp. 207–258. Computational Mechanics.

Channel, P. J. & Scovel, C. 1990 Symplectic integration of Hamiltonian systems. *Nonlinearity* **3**, 231–259.

Craik, A. D. D. 1986 *Wave Interactions and Fluid Flows*. Cambridge University Press.

Crawford, D. R., Lake, B. M., Saffman, P. G. & Yuen, H. C. 1981 Stability of weakly nonlinear deep water waves in two and three dimensions. *J. Fluid Mech.* **105**, 177–191.

Crawford, D. R., Saffman, P. G. & Yuen, H. C. 1980 Evolution of a random inhomogeneous field of nonlinear deep-water gravity waves. *Wave Motion* **2**, 1–16.

Dold, J. W. 1992 An efficient surface-integral algorithm applied to unsteady gravity waves. *J. Comput. Phys.* **103**, 90–115.

Dold, J. W. & Peregine, D. H. 1986 An efficient boundary-integral method for steep unsteady water waves. In *Numerical Methods for Fluid Dynamics II* (ed. K. W. Morton & M. J. Baines), pp. 671–679. Oxford University Press.

Dommermuth, D. G. & Yue, D. K. P. 1987 A high-order spectral method for the study of nonlinear gravity waves. *J. Fluid Mech.* **184**, 267–288.

Kartashova, E. A. 1991 On properties of weakly nonlinear wave interations in resonators. *Physica* D **54**, 125–134.

Krasitskii, V. P. 1994 On reduced Hamiltonian equations in the nonlinear theory of water surface waves. *J. Fluid Mech.* **272**, 1–20.

Krasitskii, V. P. & Kalmykov, V. A. 1993 Four-wave reduced equations for surface gravity waves. *Izv. Atmos. Ocean. Phys.* **29**, 222–228.

Longuet-Higgins, M. S. & Cokelet, E. D. 1976 The deformation of steep surface waves on water. I. A numerical method of computation. *Proc. R. Soc. Lond.* A **350**, 1–26.

McLean, J. W. 1982 Instabilities of finite-amplitude water waves. *J. Fluid Mech.* **114**, 315–330.

Newell, A. C., Passot, T. & Lega, J. 1993 Order parameter equations for patterns. *Ann. Rev. Fluid Mech.* **25**, 399–453.

Pushkarev, A. N. & Zakharov, V. E. 1998 Turbulence of capillary waves – theory and numerical simulation. In *Nonlinear Ocean Waves* (ed. W. Perrie). Advances in Fluid Mechanics, vol. 17, pp. 111–131. Computational Mechanics.

Rasmussen, J. H. & Stiassnie, M. 1999 Discretization of Zakharov's equation. *Eur. J. Mech.* B/*Fluids* **18**, 353–364.

Sanz-Serna, J. M. & Calvo, M. P. 1994 *Numerical Hamiltonian Problems*. Chapman & Hall.

Shemer, L., Jiao, H.-Y., Kit, E. & Agnon, Y. 2001 Evolution of a nonlinear wave field along a tank: experiments and numerical simulations based on the spatial Zakharov equation. *J. Fluid Mech.* **427**, 107–129.

Shemer, L. & Stiassnie, M. 1985 Initial instability and long-time evolution of Stokes waves. In *The Ocean Surface* (ed. Y. Toba & H. Mitsuyasu), pp. 51–57. D. Reidel.

Shrira, V. I., Badulin, S. I. & Kharif, C. 1996 A model of water wave 'horse-shoe' patterns. *J. Fluid Mech.* **318**, 375–404.

Shrira, V. I., Badulin, S. I. & Voronovich, A. G. 2001 EM scattering from sea surface in the presence of wind wave patterns. Part 1. *Intl J. Remote Sensing* (submitted).

Stiassnie, M. & Shemer, L. 1984 On modifications of the Zakharov equation for surface gravity waves. *J. Fluid Mech.* **143**, 47–67.

Stiassnie, M. & Shemer, L. 1987 Energy computations for evolution of class I and class II instabilities of Stokes waves. *J. Fluid Mech.* **174**, 299–312.

Su, M.-Y., Bergin, M., Marler, P. & Myrick, R. 1982 Experiments on non-linear instabilities and evolution of steep gravity wave trains. *J. Fluid Mech.* **124**, 45–72.

Tanaka, M. 2001 A method of studying nonlinear random field of surface gravity waves by direct numerical simulation. *Fluid Dyn. Res.* **28**, 41–60.

Tsai, W. & Yue, D. K. P. 1996 Computation of nonlinear free-surface flows. *Annu. Rev. Fluid Mech.* **28**, 249–278.

West, B. J. 1992 Resonant triads in ocean waves: oceanographic chaos. In *Nonlinear Dynamics of Ocean Waves* (ed. A. Brandt, S. E. Ramberg & M. F. Shlesinger), pp. 1–18. World Scientific.

West, B. J., Brueckner, K. A., Janda, R. S., Milder, D. M. & Milton, R. L. 1987 A new numerical method for surface hydrodynamics. *J. Geophys. Res.* **92**, 11803–11824.

Yuen, H. C. & Lake, B. M. 1982 Nonlinear dynamics of deep-water gravity waves. *Adv. Appl. Mech.* **22**, 67–229.

Zakharov, V. E. 1968 Stability of periodic waves of finite amplitude on the surface of a deep fluid. *J. Appl. Mech. Tech. Phys.* (USSR) **9**, 86–94.